

CALCIUM SULFITE HEMIHYDRATE DISSOLUTION AND CRYSTALLIZATION

by

CHII-HUEI PHILIP TSENG, B.S., M.S.

DISSERTATION

Presented to the Faculty of the Graduate School of

The University of Texas at Austin

in Partial Fulfillment

of the Requirements

for the Degree of

DOCTOR OF PHILOSOPHY

THE UNIVERSITY OF TEXAS AT AUSTIN

August, 1984

ACKNOWLEDGEMENTS

I would like to express my deep appreciation to my advisor, Dr. Gary T. Rochelle, for his superior leadership and personal efforts; to all my committee members for their many suggestions and advice; to Dr. Michael Schmerling, Dr. Steve Swinnea, Dr. Frank Meserole, and Dr. David Presser for their guidance with the experimental work in SEM, X-ray and IR.

Special thanks are given to my family for their constant encouragement and kind inspiration throughout my studies.

Finally, I wish to thank Mr. Pui K. Chan, his assistance and our many discussions on modeling work will be sorely missed.

Chii-Huei Philip Tseng

The University of Texas at Austin
August, 1984

ABSTRACT

Experiments were conducted to measure the dissolution and crystallization rates of calcium sulfite hemihydrate in aqueous solutions typical of flue gas desulfurization processes. A stagnant mass transfer model integrated with solution equilibrium was developed to predict $\text{CaSO}_3 \cdot 1/2\text{H}_2\text{O}$ dissolution rates as a function of pH, temperature, solution composition, and particle size. Both dissolution rate and crystal growth rate were inhibited by dissolved sulfate. The crystal growth rate per unit BET surface area, R^i (mole/cm²-min), is given by: $9.7 \times 10^{-4} \exp(-10250/RT) \times (RS_{\text{CaSO}_3} - 1)^2 \times RS_{\text{CaSO}_4}^{-1}$, where RS_{CaSO_3} and RS_{CaSO_4} are the relative saturations with respect to calcium sulfite ($\text{CaSO}_3 \cdot 1/2\text{H}_2\text{O}$) and gypsum ($\text{CaSO}_4 \cdot 2\text{H}_2\text{O}$), respectively. Scanning electron microscopy and infrared spectroscopy demonstrated that solids generated in the presence of dissolved sulfate contained solid solution sulfate and crystallized as agglomerates of very thin platelets. In the absence of solid or dissolved sulfate, the solids were agglomerates of well-formed columnar, hexagonal crystals.

TABLE OF CONTENTS

Acknowledgements	iv
Abstract	v
Table of Contents	vi
 Chapter 1. Background of Research	 1
1.1. Sulfur Dioxide Removal	1
1.2. An Overview of Flue Gas Desulfurization Processes	5
1.3. Development of FGD Technologies	8
1.3.1. Simple Wet Slurry Scrubbing	8
1.3.2. Magnesium or Organic Acid-Enhanced Limestone Slurry Scrubbing	10
1.3.3. Clear Solution Scrubbing Processes	10
1.3.4. Dry Processes	11
1.3.5. Regenerable Scrubbing Processes	15
1.4. Concept of Process Synthesis – Morphological Analysis .	15
1.5. Scope of Investigation	19
1.6. Literature Cited	22
 Chapter 2. Solid Synthesis and Characterization	 28
2.1. Summary	28
2.2. Conclusions and Significance	30
2.3. X-ray Diffraction	30
2.4. Differential Scanning Calorimetry (DSC)	32
2.5. Iodometric Titration	34
2.6. Infrared (IR) Spectroscopy	35
2.7. Coulter Counter Particle Size Distribution	40
2.8. BET Surface Area Measurement	42
2.9. Scanning Electron Microscopy (SEM)	44
2.10. Literature Cited	50
 Chapter 3. Dissolution Rate of Calcium Sulfite Hemihydrate	

in Flue Gas Desulfurization Processes	53
3.1. Summary	53
3.2. Conclusions and Significance	54
3.3. Introduction	55
3.4. Theory	59
3.4.1. Effect of Solution Composition	59
3.4.2. Effect of Particle Size Distribution	66
3.5. Experimental	68
3.5.1. Dissolution Rate Measurement	68
3.5.2. Synthesis and Characterization of Calcium Sulfite Samples	71
3.5.3. Experimental rate constant determination	71
3.6. Results and Discussion	72
3.6.1. Effect of Particle Size/Shape and Sulfate Content in Solids	74
3.6.2. Effect of temperature	75
3.6.3. Effect of pH and Dissolved Sulfite	78
3.6.4. Effect of Dissolved Sulfate	78
3.6.5. Effect of Ionic Environment and Ca^{++} Concentration	81
3.7. Nomenclature	86
3.8. Literature Cited	88
 Chapter 4. CaSO_3 Crystal Growth Rate and Crystal Habit	 93
4.1. Summary	93
4.2. Conclusions and Significance	94
4.3. Introduction	95
4.4. Experimental	99
4.4.1. Seed Crystal Synthesis and Characterization	99
4.4.2. Crystal Growth Rate Measurement	99
4.5. Results and Discussion: Growth Rate	104
4.5.1. Growth Rate Correlation	107
4.5.2. Effect of Gypsum Saturation	107
4.5.3. Effect of Temperature, Dissolved Sulfate and Seed Crystal Variation	107
4.5.4. Effects of pH, Solution Composition, Temperature, and Ionic Strength	109
4.6. Results and Discussion: Crystal Habit	111
4.6.1. Effect of Gypsum Saturation	112
4.6.2. Seed Crystal Variation	114
4.6.3. Effect of Solution Composition, Temperature and Ionic Strength	114
4.7. Nomenclature	118
4.8. Literature Cited	119

Chapter 5. Conclusions and Recommendations	124
5.1. Conclusions	124
5.2. Recommendations for Further Work	127
Appendix A. X-ray Powder Diffraction Patterns of The $\text{CaSO}_3 \cdot 1/2\text{H}_2\text{O}$ Seed Crystals	129
Appendix B. Literature Values of The X-ray Powder Diffraction Patterns of Some Calcium Sulfite and Calcium Sulfate Compounds	132
Appendix C. Derivation of The Stagnant Mass Transfer Model Surrounding A Single Particle	135
Appendix D. Tabulation of CaSO_3 Dissolution Rate Data	137
Appendix E. Tabulation of CaSO_3 Crystal Growth Rate Data in The Presence of Dissolved Mg^{++}	143
Appendix F. Apparent pKa Values of HSO_3^- in Aqueous Solutions Typical of FGD Processes	145

LIST OF TABLES

Table 1-1:	Estimated Emissions of Sulfur Dioxide	2
Table 1-2:	Description of Some Sulfur Dioxide Removal Processes	6
Table 2-1:	Summary of CaSO_3 Solids Preparation and Characterization	29
Table 2-2:	CaSO_3 Particle Size Distributions	41
Table 3-1:	Diffusivities at 25 °C	63
Table 3-2:	Adjusted Sh and K_{sp} of $\text{CaSO}_3 \cdot 1/2\text{H}_2\text{O}$ as a Function of Solid Sulfate Content and Temperature	75
Table 4-1:	CaSO_3 Seed Crystals	100
Table 4-2:	Corrected Values of K_{sp} of $\text{CaSO}_3 \cdot 1/2\text{H}_2\text{O}$ as a Function of Temperature and Solid Sulfate Content	101
Table 4-3:	CaSO_3 Crystal Growth Rate	105

Chapter 1

Background of Research

One of the most abundant air pollutants emitted in the United States is sulfur dioxide (SO_2). It was estimated that more than 30 million tons of SO_2 was discharged into the U.S. atmosphere in 1977 (Wark and Warner, 1981). Over half of these SO_2 emissions came from stacks of electric power generating plants operating on sulfur-containing coal and oil, as can be seen in Table 1-1.

1.1 Sulfur Dioxide Removal

In this country, the use of sulfur-containing fossil fuels doubles about every 20 years (Crynes, 1977). If corrective measures are not taken, the annual emission of SO_2 into the U.S. atmosphere by the year 2000 is expected to be in excess of 250 billion pounds, 80 percent of which will result from burning fossil fuels (Chilton, 1971).

SO_2 emission into the atmosphere causes many problems. It has been known that vegetation will grow slower or not at all in an atmosphere polluted with large amounts of sulfur dioxide. According

Table 1-1: Estimated Emissions of Sulfur Dioxide

(million tons/year)

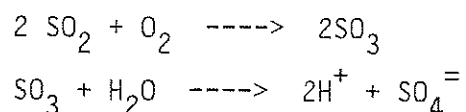
Source	1971	1974	1977
Transportation	0.7	0.7	0.8
Stationary fuel combustion			
Electric utilities	15.7	17.2	17.6
Industrial	4.0	3.3	3.2
Residential, commercial	1.9	1.6	1.6
Chemical industry	2.0	2.1	1.8
Metals industry	3.8	3.5	2.4
Others	0.2	0.	0.
Total	28.3	28.4	27.4

* Source: National Air Quality, Monitoring, and Emissions Trends Report, 1977, EPA-450/2-78-052, December 1978.

to a recent World Watch Institute study, it was found that 9 million acres of forests in Europe and the eastern U.S. now show damage that can be linked to air pollution (Chemical & Engineering News, April 9, 1984).

Sulfur dioxide is harmful to mankind, too. Several air pollution disasters occurred recently - Meuse Valley, Belgium, 1930; Donora, Pennsylvania, 1948; New York City, 1953 and 1963; London, England, 1952 and 1962, etc. (Houghson, 1966). A great number of people became sick and many died.

Sulfur dioxide emitted into the atmosphere also causes the most serious and ever-growing acid rain problem via the following chemical reactions (Matteson, 1969; Bufalini, 1971; Seinfeld, 1975):



Since there is no way to alter the results of acid rain once it has occurred in a region, the only solution to this problem is to reduce the SO_2 emissions at the sources. Several possible methods or alternatives may be used to reduce SO_2 emissions from fossil-fuel combustion. These potential methods are (Crynes, 1977; Rochelle, 1977):

- change to low-sulfur fuels;
- use desulfurized coal and oil;
- remove SO_2 from flue gases;
- build tall stacks to improve atmospheric dispersion;
- generate power by nuclear reactors.

Among these, low-sulfur fuels are expensive and not readily available in many areas. Desulfurization of fuels is also expensive, and the technology for desulfurizing coal is still in the development stage. Building tall stacks to help disperse SO_2 in the atmosphere reduces air pollution in the local area effectively, but the SO_2 never disappears and will remain in the atmosphere permanently, or be absorbed in cloud water and rain drops and causes the acid rain problem - probably in some areas a thousand miles away. Nuclear reactors for power generation are clean, but the technology of the economic breeder-type reactor has not been well-developed so far, the Three-Mile Island accident had brought the security problems to public concern, and the safe storage of nuclear fuel waste has not been solved. Therefore, the solution that appears to be of most immediate application is removal of SO_2 from stack gases.

1.2 An Overview of Flue Gas Desulfurization Processes

Over sixty processes have been developed for removal of SO_2 from utility stack gases, and several of these processes are being commercially used (Crynes, 1977; Rochelle, 1982; Laseke, et al., 1983; Ando, 1983). Flue gas desulfurization technology must perform several important functions: (1) It must remove sulfur dioxide from the flue gas effectively; (2) It must dispose of the sulfur product by marketing or by environmentally acceptable waste disposal; and (3) It must be able to operate reliably without frequent shut-down (Cornell and Dahlstrom, 1973; Rochelle, 1977).

Sulfur dioxide removal processes may be grouped according to two classifications: (1) throwaway or regenerable; and (2) wet or dry. Throwaway scrubbing processes remove the sulfur dioxide by contact with an aqueous alkali solution and dispose of it as a calcium sulfite/sulfate solid waste. As a result, fresh chemicals such as lime or limestone must be continually added for neutralization. In regenerable processes, the chemistry is such that the removal agents can be continually regenerated in a closed-loop system so that no fresh alkali chemicals need to be continually added. Wet or dry processes differ simply by whether or not the active removal agent is contained in a liquid solution.

A brief comparison of some of the major processes for SO_2 removal from flue gases are listed in Table 1-2 (Wark and Warner,

1981). The processes listed in the table can be divided into three classes: throwaway and regenerative - both of which are wet scrubbing processes, and dry processes. Since sulfur dioxide is an acid gas, almost all of the scrubbing processes use an aqueous solution or a slurry of some alkali. The throwaway processes usually dispose of the removed sulfur in some form of calcium-type sludge, for example, calcium sulfite hemihydrate or calcium sulfate dihydrate (gypsum). As a result, the required alkali makeup to continually feed into the processes is considerable. The product of the regenerative processes is usually elemental sulfur or sulfuric acid, and the alkali makeup is recycled (Koehler, 1974; Leckner, et al., 1982; Rochelle, 1982). Hence little makeup of alkali chemicals is required in regenerative processes. Throwaway processes generally can be used to remove the SO_2 as well as the particulate in the flue gas, such as fly ash. On the other hand, regenerative processes usually need a high efficiency particulate collector, such as an electrostatic precipitator (ESP), to precede the SO_2 removal equipment because particulates are not acceptable in the operations.

Dry processes are quite attractive because they generally have low capital costs and are simple to design, install, and operate (Shah, 1982; Reisdorf, 1983). Low lime or limestone utilization is a serious disadvantage for dry processes (Palazzolo, et al., 1983). Therefore, improving limestone or lime utilization presents the major opportunity for dry processes (Ruiz-Alsop, 1984).

1.3 Development of FGD Technologies

1.3.1 Simple Wet Slurry Scrubbing

The earliest FGD process used in the world was lime/limestone wet scrubbing, originally developed in England by Imperial Chemical Industries (ICI) in the 1930s. As shown in Figure 1-1, this process reacts limestone (CaCO_3) or lime (CaO) with the flue gas in an aqueous slurry system to produce CaSO_3 . Because most waste gases contain oxygen, the solids will also contain variable quantities of CaSO_4 depending on the oxygen to SO_2 ratio (Rochelle and King, 1978).

The design of this system is constrained primarily by the need to avoid CaSO_3 and CaSO_4 scaling in the scrubber. The combination of crystallizer residence time and CaSO_4 solids concentration must be sufficient to desupersaturate the scrubber feed. The liquid circulation rate must be adequate to avoid excessive CaSO_4 supersaturation at the scrubber exit. CaSO_3 scaling is avoided by limiting the amount of unreacted CaCO_3 or CaO solid that is returned to the scrubber (Rochelle, 1982).

1.3.2 Magnesium or Organic Acid-Enhanced Limestone Slurry Scrubbing

The use of limestone, instead of lime, in calcium-based wet scrubbers is economically preferable because of the increasing cost difference between limestone and lime. However, the economic advantage of using limestone is diminished if its utilization in a particular process is low. It has been known that the dissolution of limestone is controlled by the diffusion of ions in solutions (Chan and Rochelle, 1982). Therefore, the simple limestone slurry scrubbing process can be modified by adding some soluble additives, such as organic acids or magnesium salts, into the scrubbing solution to enhance the mass transfer performance (Cronkright and Leddy, 1976; Rochelle and King, 1977; Weismantel, 1978; Rochelle, et al., 1982; Sada, et al., 1981, 1983; Laslo, et al., 1983).

1.3.3 Clear Solution Scrubbing Processes

One major problem encountered with most lime/limestone slurry scrubbing processes is the deposition of CaSO_3 and CaSO_4 solids on scrubber internals and the mist eliminator. To achieve high reliability, no solids must be deposited in the scrubber that would require an early shut-down for cleaning purposes. This means that a clear scrubbing liquor having only minor amounts of fly ash would be advantageous. In this way, deposits from slurries such as that found in limestone scrubbing would be eliminated. Therefore, single alkali scrubbing which uses a clear liquor such as sodium hydroxide was developed (Slack, 1973).

Figure 1-2 is a flowsheet of a typical dual-alkali process which combines the philosophies of both throwaway and regenerative technologies, and keeps the advantages of the clear solution processes. A soluble alkali, sodium hydroxide, is used to scrub the flue gas to remove SO_2 . The use of sodium hydroxide scrubbing liquor means a clear solution having only minor amounts of flyash included in the circulated stream. The use of sodium hydroxide scrubbing liquor also results in a minimum equilibrium vapor pressure of SO_2 over the solution. Therefore, the driving force then becomes the actual SO_2 concentration of the gas and the absorption rate is maximized, which results in a high SO_2 removal efficiency (Cornell and Dahlstrom, 1973). The scrubbing solution exits from the scrubber subsequently enters a second alkali loop to react with lime or limestone and produces a solid calcium sulfite/sulfate waste outside the scrubber as well as a regenerated sodium scrubber feed solution. Therefore, the only consumption of alkali makeup is the cheaper lime or limestone, and the only discharge from such a system would be the dewatered precipitated calcium solids and the scrubbed clean flue gas (LaMantia, et al., 1974; Glancy, et al., 1983).

1.3.4 Dry Processes

Even though wet scrubbing technology has been commercially proven, process reliability has often been disappointing. Corrosion, erosion, plugging, scaling and freezing have been identified as major problems with wet-scrubber systems (Syrett, 1983). Because most of

the wet scrubber problems relate to the use of circulating acid water slurries, spray dryer technology has been introduced to reduce water requirements by about one half (Shah, 1982). In the spray-drying process, an alkaline solution or slurry is sprayed into the flue gas stream. The sprayed material reacts with SO_2 and at the same time water evaporates (from the heat of the flue gas) resulting in dry waste. The dried material also reacts with the SO_2 during collection in the particulate control device (Gustke, et al., 1983; Reinauer, et al., 1983).

Spray dryer technology appears more promising than wet scrubbing, but a number of questions concerning the reliability of the processes remain unanswered. These questions relate to reheat requirements and plugging, scaling and corrosion problems resulting from the use of water (Blythe and Rhudy, 1983).

Dry-scrubbing processes carry spray-drying philosophy one step further by eliminating water usage entirely. In a dry-scrubbing process, a dry alkaline powder, typically sodium bicarbonate, is injected directly into the flue gas stream, as shown in Figure 1-3. The alkaline particles react with SO_2 while suspended in the gas stream. Dry waste product from this reaction is subsequently collected in a particulate collection device (baghouse, precipitator, etc.) and the clean flue gas is vented to the atmosphere. Additional reaction between alkaline particles captured in the particulate

control equipment and SO_2 occurs as the flue gas passes through the particulate control equipment (Shah, 1982).

1.3.5 Regenerable Scrubbing Processes

Regenerable processes remove SO_2 from stack gases and convert it to marketable products such as elemental sulfur, sulfuric acid, liquid sulfur dioxide and ammonium phosphate (Koehler, 1974; Chi, et al., 1982; Leckner, et al., 1982). Such systems are environmentally attractive because they avoid the production of waste products and economically attractive because they avoid the cost of alkali makeup and solid waste disposal. However, the energy required for processing and the complexity of the processing usually make these processes more expensive than throwaway scrubbing (Rochelle, 1982). A large number of regenerable scrubbing processes have been conceived and partially developed. Among these, the Wellman-Lord and MgO processes are commercially significant (Leseke, et al., 1983; Reisdorf, et al., 1983) Figure 1-4 is a typical flowsheet of the MgO process.

1.4 Concept of Process Synthesis - Morphological Analysis

Given a basic process concept or objective, process synthesis is the first step of process design. It may precede or be parallel to process development. Morphological synthesis defines new process alternatives by decomposing existing process concepts or objectives

into subsets on the basis of unit operations, functions, or reactant alternatives. New processes are then defined by the combination of one alternative from each subset. Ideally, morphological synthesis could achieve preliminary process evaluation by combining the best elements of each subset. In practice, it is usually difficult to define the subsets in a manner that avoids interactions or synergistic effects. However, morphological synthesis does highlight the interactions and permit a better preliminary evaluation of the numerous alternatives (Rochelle, 1977).

In this section, the concept of morphological synthesis is used to describe the development and innovations of various FGD technologies. As can be seen in Figure 1-5, several major FGD processes are linked with each other by some common design philosophies. The new, more advanced FGD technologies can be expected or developed if some breakthrough can be made via extensive research or pilot plant study.

The dissolution and crystallization of calcium sulfite/sulfate affects the composition and chemical equilibria of the scrubbing solutions. Therefore, it affects SO_2 absorption, lime or limestone utilization and sulfite oxidation in the scrubber and hold tank. The modification of $\text{CaSO}_3/\text{SO}_4$ crystal habit also determines the ease of dewatering of the solid products, thus the operating cost of filtration, the loss of alkali chemical makeup, and the economics of waste disposal.

Hence $\text{CaSO}_3/\text{SO}_4$ dissolution and crystallization has become a key factor which is central to the development of FGD technologies that use calcium based alkali chemicals, such as lime or limestone, to neutralize the scrubbing solutions. A thorough understanding of this phenomenon will help solve the problems met in modifying current processes or developing new, advanced processes. For example, it is economically attractive to convert a dual alkali FGD system from lime to limestone due to the significant cost difference between these two chemicals. However, the obstacles which currently hinder the dual alkali technologies from being developed a step further is that a high soda ash consumption and a poor settleability of the solid products have been observed in a recent limestone dual alkali pilot plant study. And the key solution to this problem is the better understanding of calcium sulfite/sulfate dissolution and crystallization in the scrubbing liquors.

1.5 Scope of Investigation

There are three major objectives of this work:

- to measure and model CaSO_3 dissolution rates;
- to measure and model CaSO_3 crystal growth rates;
- to study CaSO_3 crystal habit.

Three batches of calcium sulfite seed crystals were synthesized in the laboratory by reacting CaCl_2 solution with

$\text{Na}_2\text{SO}_3/\text{Na}_2\text{SO}_4$ solution at a solution composition super-saturated with respect to calcium sulfite. These solids were characterized using iodometric titration, differential scanning calorimetry, X-ray powder diffraction, scanning electron microscopy, infrared spectroscopy, BET surface area measurement, and Coulter Counter particle size analysis.

The pH-stat method has been applied to the rate measurement of CaSO_3 dissolution and crystal growth by monitoring the pH change due to the shift in the $\text{SO}_3^{=}$ - HSO_3^- equilibrium which was caused by the dissolution or crystallization of CaSO_3 solids. The same seed crystals were used in both dissolution and crystallization experiments, and the effects of pH, solution composition, temperature and seed crystals were studied.

A stagnant mass transfer model has been developed to simulate the ionic mass transfer surrounding a single particle. Solution equilibria and $\text{CaSO}_3/\text{CaSO}_4$ supersaturation were calculated from the Bechtel-modified Radian solution equilibrium program. Two adjustable parameters were used in the model to account for the CaSO_3 solubility correction and the enhancement of mass transfer coefficient due to the deviations of particle size/shape from the conditions suitable for a stagnant model. Crystal growth rates were correlated as a function of calcium sulfite and gypsum saturation.

Finally, the grown crystals in crystallization experiments

were recovered and examined under a scanning electron microscope to observe the change in crystal morphology. Infrared spectroscopy was also used to determine the solid composition of the grown crystals as a function of the mother liquor composition.

1.6 Literature Cited

1. Ruiz-Alsop, R. "Reaction of SO_2 with Ca(OH)_2 ", Ph.D. Dissertation, University of Texas at Austin (1984)
2. Ando, J. "Status of SO_2 and NO_x Removal in Japan", Presented at the EPA/EPRI Symposium on Flue Gas Desulfurization, New Orleans, November 1 - 4, 1983
3. Blythe, G.M. and R.G. Rhudy "EPRI Spray Dryer/Baghouse Pilot Plant Status and Results", Presented at the EPA/EPRI Symposium on Flue Gas Desulfurization, New Orleans, November 1 - 4, 1983
4. Brandt, C.S. and W.W. Heck "Effects of Air Pollutants on Vegetation", in A.C. Stern (editor) "Air Pollution", 1, Academic Press, New York (1968)
5. Bufalini, M. "The Oxidation of Sulfur Dioxide in Polluted Atmospheres: A Review", Environ. Sci. Tech. 5, 685 (1971)
6. Chi, C.V., Peck, R.E., Tavakoli, F., and D.T. Wasan "The IIT Flue Gas Desulfurization Process", Chem. Eng. Prog., 78 (1), 78 - 82 (1982)
7. Chilton, T.H. "Reducing SO_2 Emission from Stationary Sources", Chem. Eng. Prog., 67 (5), 69 - 72 (1971)

8. Cornell, C.G. and D.A. Dahlstrom "Sulfur Dioxide Removal in a Double-Alkali Plant", Chem. Eng. Prog., 69 (12), 48 - 54 (1973)
9. Cronkright, W.A. and W.J. Leddy "Improving Mass Transfer Characteristics of Limestone Slurries by Use of Magnesium Sulfate", Environ. Sci. Tech., 10, 569 (1976)
10. Crynes, B.L. "Chemical Reactions as a Means of Separation; Sulfur Removal", Chem. Proc. & Eng. Ser., 11, Marcel Dekker, Inc., New York (1977)
11. Glancy, D.L., Grant, R.J., Legatski, L.K., Wilhelm, J.H. and B.A. Wrobel "Utility Double Alkali Operating Experience", Presented at the EPA/EPRI Symposium on Flue Gas Desulfurization, New Orleans, November 1 - 4, 1983
12. Houghson, R.V. "Controlling Air Pollution", Chem. Eng., 71 - 90, August 29, 1966
13. Koehler, G.R. "Alkaline Scrubbing Removes Sulfur Dioxide", Chem. Eng. Prog., 70 (6), 89 - 91 (1974)
14. LaMantia, C.R., Lunt, R.R. and I.S. Shah "Dual Alkali Process For Sulfur Dioxide Removal", Chem. Eng. Prog., 70 (6), 92 - 93 (1974)

15. Laseke, B.A., Melia, M.T. and N. Kaplan "Trends in Commercial Applications of FGD", Presented at the EPA/EPRI Symposium on Flue Gas Desulfurization, New Orleans, November 1 - 4, 1983
16. Laslo, D., Chang, J.C.S. and J.D. Mobley "Pilot Plant Tests on The Effects of Dissolved Salts on Lime/Limestone FGD Chemistry", Presented at the EPA/EPRI Symposium on Flue Gas Desulfurization, New Orleans, November 1 - 4, 1983
17. Leckner, P., Pearson, R.O. and R.T. Wood "The Wellman-Lord SO₂ Recovery Processes", Chem. Eng. Prog., 78 (1), 65 - 70 (1982)
18. Matteson, M.J., Stober, W., and H. Luther "Kinetics of The Oxidation of Sulfur Dioxide by Aerosols of Manganese Sulfate", Ind. & Eng. Chem. Fundam., 8, 677 - 687 (1969)
19. Meserole, F.B., Glover, R.L. and D.A. Stewart "Studies of The Major Factors Affecting Magnesium Limestone Dissolution", ACS Symp. Ser., 188, 99 - 111 (1982)
20. Palazzdo, M.A., Brna, T.G. and M.E. Kelly "Current Status of Dry SO₂ Control Systems", Presented at the EPA/EPRI

Symposium on Flue Gas Desulfurization, New Orleans,
November 1 - 4, 1983

21. Reinauer, T.V., Monat, J.P. and M. Mutsakis "Dry FGD on an Industrial Boiler", Chem. Eng. Prog., 79 (3), 74 - 81 (1983)
22. Reisdorf, J.B., Keeth, R.J., Miranda, J.E., Scheck, R.W. and T.M. Morasky "Economic Evaluation of FGD Systems", Presented at the EPA/EPRI Symposium on Flue Gas Desulfurization, New Orleans, November 1 - 4, 1983
23. Rochelle, G.T. "Process Synthesis and Innovation in Flue Gas Desulfurization", EPRI FP-463-SR Special Report, (1977)
24. Rochelle, G.T. and C.J. King "The Effect of Additives on Mass Transfer in CaCO_3 or CaO Slurry Scrubbing of SO_2 from Waste Gases", Ind. & Eng. Chem. Fundam., 16, 67 - 75 (1977)
25. Rochelle, G.T. and C.J. King "Alternatives for Stack Gas Desulfurization By Throwaway Scrubbing", Chem. Eng. Prog., 74 (2), 65 - 70 (1978)

26. Rochelle, G.T. "Desulfurization, Gas, Stack Gas", in J.J. McKetta (editor) "Encyclopedia of Chemical Technology", 15, 145 - 163 (1982)
27. Rochelle, G.T., Weems, W.T., Smith, R.J. and M.W. Hsiang "Buffer Additives for Lime/Limestone Slurry Scrubbing", ACS Symp. Ser., 188, 243 - 265 (1982)
28. Sada, E., Kumazawa, H., Sawada, Y. and I. Hashizume "Kinetics of Absorptions of Lean Sulfur Dioxide into Aqueous Slurries of Calcium Carbonate and Magnesium Hydroxide", Chem. Eng. Sci., 36, 149 - 155 (1981)
29. Sada, E., Kumazawa, H., Hashizume, I. and N. Kamishima "Desulfurization by Limestone Slurry with Added Magnesium Sulfate", Chem. Eng. J., 22, 133 - 141 (1981)
30. Sada, E., Kumazawa, H. and H. Nishimura "Absorption of Sulfur Dioxide into Aqueous Double Slurries Containing Limestone and Magnesium Hydroxide", AIChE J., 29, 60 - 65 (1983)
31. Seinfeld, J.H. "Air Pollution; Physical and Chemical Fundamentals", McGraw-Hill, Inc., New York (1975)

32. Shah, N.D., "Dry Scrubbing of SO_2 ", Chem. Eng. Prog., 78, (6) 43 - 46 (1982)
33. Slack, A.V. "Removing SO_2 from Stack Gases", Environ. Sci. Tech., 7, 110 (1973)
34. Syrett, B.C. "EPRI Spray Dryer/Baghouse Pilot Plant Status and Results", Presented at the EPA/EPRI Symposium on Flue Gas Desulfurization, New Orleans, November 1 - 4, 1983
35. Wark, K. and C.F. Warner "Air Pollution; Its Origin and Control", Second edition, Harper & Row, Publishers, New York (1981)
36. Weismantel, G.E. "Limestone + Magnesium : A New SO_2 Control Team", Chem. Eng., 111 - 114, September 11, 1978

Table 2-1: Summary of CaSO_3 Solids Preparation and Characterization

Sample No.	1	3	5
Synthesis Method	1 M Na_2SO_3 into 1 M CaCl_2	1.35 M Na_2SO_3 , 0.15 M Na_2SO_4 into 1 M CaCl_2	2 M CaCl_2 into 2 M Na_2SO_3
CaSO_4 Concentration in Solids (Mole %)			
Iodometric Titration	5.1	10.6	3.0
Infrared Spectroscopy	3.4	10.7	1.0
Particle Size (μm)	22 ± 10	12 ± 10	25 ± 10
Platelet Thickness (μm)	0.1	0.01	2
BET Surface Area (m^2/g)	1.92	9.54	1.23

2.2 Conclusions and Significance

1. Solids are $\text{CaSO}_3 \cdot 1/2\text{H}_2\text{O}$ with solid solution of CaSO_4 (no other CaSO_3 or CaSO_4 phases have been observed).
2. The calcium sulfite solids are agglomerates of crystals. The typical particle sizes are 10 - 25 μm .
3. Platelet thickness is a strong function of sulfate content. Low sulfate content gives bulkier crystals.

2.3 X-ray Diffraction

As shown in Figure 2-1, the X-ray powder diffraction pattern identifies only one crystalline structure of calcium sulfite hemihydrate ($\text{CaSO}_3 \cdot 1/2\text{H}_2\text{O}$) in sample 1. The other samples give similar results (Appendix A). The diffraction pattern is consistent with the literature values as listed in Appendix B (Scheib, et al. 1974). The calcium sulfite crystalline structure has four major peaks in its X-ray diffraction patterns. The d-spacings of these four major peaks are 3.16, 3.81, 5.35 and 5.56 Å which correspond to diffraction angles of 28.1° , 23.3° , 16.5° , and 15.9° respectively. Peaks are also found at these positions in the X-ray diffraction patterns of the synthesized solids. No crystalline structures of calcium sulfate hemihydrate ($\text{CaSO}_4 \cdot 1/2\text{H}_2\text{O}$) or calcium sulfate dihydrate ($\text{CaSO}_4 \cdot 2\text{H}_2\text{O}$) have been identified, confirming that no pure

sulfate phases exist in the calcium sulfite solids. The literature values of the X-ray diffraction patterns of closely related calcium sulfite and calcium sulfate compounds are listed in Appendix B for comparison.

2.4 Differential Scanning Calorimetry (DSC)

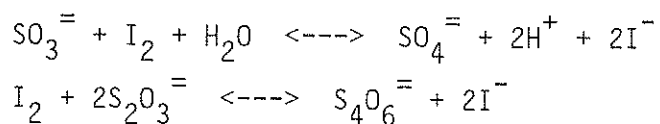
DSC was used to characterize the calcium sulfite solids by monitoring the enthalpy change as a function of temperature. The phase changes would be marked by rapid changes in the heat capacity, in the temperature ranges of 120 - 140 °C for gypsum; 150 - 170 °C for calcium sulfate hemihydrate; and 350 - 430 °C for calcium sulfite hemihydrate (Jones, et al., 1976). These heat capacity changes are associated with the loss of hydrated water in the calcium sulfite solids.

A typical DSC scan of the synthesized calcium sulfite solids is shown in Figure 2-2. The DSC scans of other samples are similar. The change in heat capacity at about 400 °C for the samples results from the endothermic dehydration of $(\text{CaSO}_3)_x(\text{CaSO}_4)_{1-x} \cdot 1/2\text{H}_2\text{O}$ solid solutions. No gypsum ($\text{CaSO}_4 \cdot 2\text{H}_2\text{O}$) was found in the solid samples because the DSC scan shows no enthalpy change in the temperature range of 120 - 140 °C. The DSC scan also showed that no separate phase of $\text{CaSO}_4 \cdot 1/2\text{H}_2\text{O}$ exists, because no significant enthalpy change occurs in the temperature range of 150 - 170 °C. The DSC scans confirmed that the sulfate content in the solids is present as a solid solution with $\text{CaSO}_3 \cdot 1/2\text{H}_2\text{O}$.

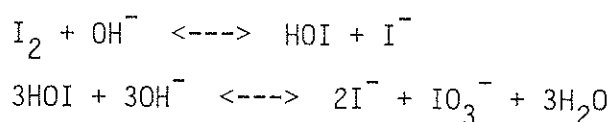
2.5 Iodometric Titration

Iodometric titration was used to determine the sulfite purity of the calcium sulfite solids. A known amount of calcium sulfite solids were dissolved in a pH 6 buffer solution, which was made by mixing 1 M sodium acetate with an equal amount of 0.05 M acetic acid. An excess of standard iodine solution was then added, and the solution was back-titrated with thiosulfate to determine the sulfite content of the calcium sulfite solids. Soluble starch was used as the indicator to find the end point of the iodometric titration. The results of iodometric titration indicated that the three batches of calcium sulfite solids have sulfite purities of 94.9, 89.4, and 97 weight percent as $\text{CaSO}_3 \cdot 1/2\text{H}_2\text{O}$ respectively.

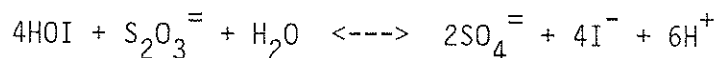
The chemistry involved in iodometric titration can be described as follows:



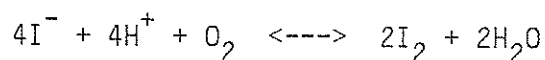
The pH 6 buffer is used in the iodometric titration to prevent the side reactions which would occur at high pH (Dick, 1973):



The hydrolysis of iodine becomes significant at a pH of about 8, with the reaction of thiosulfate and bypoidite being



thus permitting a departure from the expected stoichiometry of the iodine-thiosulfate reaction. On the other hand, iodine can be oxidized by air in the reaction:



The reaction is very slow in neutral or slightly basic media but increases in reaction rate with increasing acidity. In order to avoid those possible difficulties, titrations of iodine and sodium thiosulfate are generally conducted in solutions having a pH of about 6.

2.6 Infrared (IR) Spectroscopy

The frequencies at which a material absorbs infrared energy depends upon the internal vibrations of the molecule and hence upon its composition. The introduction of infrared spectroscopy into the field of mineral analysis has been limited due to the excellence of the X-ray diffraction technique. However, the infrared technique is quick, simple, relatively inexpensive and serve as a useful supplementary technique in the identification of mineral species.

The results of iodine titration indicated that the three batches of calcium sulfite solids have sulfite content ranging from 88 to 97 percent, but both DSC and X-ray diffraction methods failed to show the presence of a pure phase of sulfate compound. Infrared spectroscopy was used to confirm the presence of sulfate in the calcium sulfite solids.

The technique of preparing calcium sulfite samples for IR spectral analysis is as follows (Meserole, 1983): Approximately one milligram dry calcium sulfite powder is put between two KBr windows, followed by grinding the sample until the particle size of the calcium sulfite solids is the same order-of-magnitude as the wavelength of the IR sources (normally several μm). This technique prevents the inconvenience of using KBr pellet or mineral oil (nujol) methods, and provides a more accurate IR spectrum without the interference of the diluents.

The infrared spectra of the three calcium sulfite solids are shown in Figures 2-3 to 2-5. The absorption structures of interest are the major sulfite band at approximately 980 cm^{-1} and the sulfate band near 1130 cm^{-1} . The structure in the $3200 - 3600\text{ cm}^{-1}$ and $1600 - 1700\text{ cm}^{-1}$ ranges is a result of the hydrated water in the calcium sulfite/sulfate solids. The absorption bands in the $600 - 700\text{ cm}^{-1}$ region are due to the sulfite and sulfate ions but are not as distinctive as the major bands (Gadsden, 1975; Jones et al., 1976).

Relative absorbance of sulfite and sulfate in the IR spectra have been used to quantify the relative content of sulfite and sulfate ions in the calcium sulfite solids (Meserole, 1983). The sulfite content calculated by this method is reasonably consistent with that obtained from the iodine titration method, as shown in Table 2-1.

The combined results of X-ray diffraction, DSC and IR spectral analysis suggest that sulfate ion will substitute for sulfite ion in the $\text{CaSO}_3 \cdot 1/2\text{H}_2\text{O}$ crystal lattice under some crystallization conditions.

2.7 Coulter Counter Particle Size Distribution

Several methods for the measurement of calcium sulfite particle sizes had been compared in an earlier EPA report by Edwards (1979). In later research, Brecevic and Garside (1981) studied the measurement of crystal size distributions, especially in the micrometer range. Their experimental results indicated that the crystal size distribution obtained with both the Coulter Counter, which is based on the "sensing zone" principle, and the Malvern Particle Size Analyzer, which is based on the principle of forward scattering of laser light, were very similar and lend confidence to such measurements at these micrometer size ranges. Both Edwards and Brecevic's studies suggested that the Coulter Counter method is reliable and convenient in measuring calcium sulfite particle size distributions in the micrometer size range.

Table 2-2: CaSO₃ Particle Size Distributions

Effective Diameter (μm)	Volume % Between The Two Diameters		
	Sample 1	Sample 3	Sample 5
1.59	0	0	0
2.00	0.6	0.8	0
2.52	0.7	1.5	0
3.17	0.6	0.7	0
4.00	0.8	1.3	0
5.04	1.6	3.2	0
6.35	2.6	6.8	0
8.00	4.4	12.2	0.2
10.08	6.6	17.4	0.9
12.7	10.3	18.0	4.3
16.0	15.4	14.7	17.9
20.2	23.6	10.5	38.2
25.4	20.2	5.7	27.2
32.0	8.0	4.3	8.7
40.3	2.5	1.5	2.3
50.8	2.1	1.4	0.3
64.0			

The Coulter Counter method has been extensively used in some previous limestone dissolution studies (Chan, 1981; Chan and Rochelle, 1982; Toprac, 1982), and also used in the determination of crystal growth and nucleation kinetics from the steady-state crystal size distribution (CSD) in a continuous mixed suspension mixed product removal (MSMPR) crystallizer (Randolph and Larson, 1971; Etherton and Randolph, 1981; Randolph, 1980; Vaden, 1981; Kelly, 1983). It has proved to be efficient, reliable and reproducible in measuring particle size distributions in micrometer size ranges.

The particle size distributions of the calcium sulfite samples are given in Table 2-2. They were determined by a Model TA II Coulter Counter using 0.18 M CaCl_2 electrolyte with a 140 μm aperture.

2.8 BET Surface Area Measurement

The total surface area of a porous solid has traditionally been accepted to be the surface area deduced by nitrogen adsorption at low temperature using the procedure called the BET method (Brunauer, et al., 1938). This method is based on an isotherm in terms of the pressure of the adsorbing gas P , and its saturated vapor pressure P_0 . From this isotherm the monolayer volume V_m , and thus the total surface area can be estimated.

The BET equation can be written as:

$$P/V_a(P_0 - P) = 1/V_m C + P(C-1)/V_m P_0 C$$

where C is a constant, V_a is the volume of gas adsorbed at 0 °C and 760 mmHg, and V_m is volume of gas adsorbed as a monolayer at the same conditions.

The derivation of the BET equation was based on the premise of a plane uniform and unrestricted multilayer physical adsorption on top of the initial monolayer having the energetics of the liquid phase (Anderson, 1968). Given data on volume adsorbed versus pressure, the surface area of the sample can be calculated by the specified volume of gas adsorbed at the point of monolayer completion. Therefore, the BET equation provides a reliable and reproducible means to determine the total surface area (Rase, 1977).

An AccuSorb Model 2100E Physical Adsorption Analyzer was used to measure the BET surface area with N_2 of the calcium sulfite solids. The results are listed in Table 2-1. Sample 3 with high sulfate content and thinner platelets gives much higher BET surface area.

2.9 Scanning Electron Microscopy (SEM)

The SEM technique has been applied to characterize the shapes and sizes of the calcium sulfite crystals. The technique of mounting calcium sulfite crystals for SEM viewing is as follows: Approximately one milligram of calcium sulfite powder is dusted onto a thin film of graphite glue, which is on an SEM stage. It is then sputtered or vacuum-evaporated with an Au-Pd alloy to provide the necessary conducting medium for the SEM. This method yields a uniform distribution and also minimizes the possible breakage of the calcium sulfite samples.

The SEM photographs of the synthesized calcium sulfite solids are shown in Figures 2-6 to 2-12. The photographs of sample 1 (Figures 2-6 to 2-8) show "platelet-like" shape for the calcium sulfite crystals. Figure 2-6 at 600 X magnification shows the existence of both large and small particles, the sizes range from less than 1 μm to over 50 μm , in agreement with the results obtained from Coulter Counter measurement. The lengths and dimensions of the "platelet-like" crystals vary; but larger crystals are usually found in larger particles which can be used as an indirect evidence of crystal growth (Figures 2-7 and 2-8).

Figure 2-9 is the low magnification photograph of sample 3, which has 11 percent sulfate content. The particles are composed of many tiny and very thin platelet crystals, as shown in Figure 2-10.

conditions of sample 5 give large blocky crystals rather than thin platelet crystals. Later results (Chapter 4) demonstrate that the change in crystal habit results from the very low sulfate content of the solids, not from the high ratio of dissolved sulfite and calcium at the crystallization conditions. The significant differences in the crystal habit of these three CaSO_3 solids are investigated and discussed further in Chapter 4.

2.10 Literature Cited

1. Anderson, R. B. "Experimental Methods in Catalytic Research", 1, Academic Press, New York (1968)
2. Brecevic, L. and J. Garside "On the Measurement of Crystal Size Distributions in the Micrometer Size Range", Chem. Eng. Sci., 36, 867-869 (1981)
3. Brunauer, S., Emmett, P. H., and E. Teller "The Adsorption of Gases in Multimolecular Layers", J. Am. Chem. Soc., 60, 309 - 319 (1938)
4. Chan, P. K. "CaCO₃ Dissolution in SO₂ Scrubbing Solutions; Mass Transfer Enhanced by Chemical Reactions", M.S. Thesis, University of Texas at Austin (1981)
5. Chan, P. K. and G. T. Rochelle, "Limestone Dissolution; Effects of pH, CO₂, and Buffers Modeled by Mass Transfer", ACS Symp. Ser., 188, 75-97 (1982)
6. Dick, J. G. "Analytical Chemistry", McGraw-Hill, Inc. (1973)
7. Edwards, L. O. "Calcium Sulfite Crystal Sizing Studies", EPA-600/7-79-192 (1979)

8. Etherton, D. L. and A. D. Randolph "Nucleation/Growth Rate Kinetics of Gypsum in Simulated FGD Liquors: Some Process Configurations for Increasing Particle Size", AICHE Symp. Ser., 77 (211), 87-94 (1981)
9. Gadsden, J. A. "Infrared Spectra of Minerals and Related Inorganic Compounds", Butterworth & Co., Ltd., London (1975)
10. Jones, B. F., Lowell, P. S. and F. B. Meserole "Experimental and Theoretical Studies of Solid Solution Formation in Lime and Limestone SO₂ Scrubbers", EPA-600/2-76-273a (1976)
11. Kelly, B. "Study of CaSO₃·1/2H₂O Nucleation and Growth Rates in Simulated Flue Gas Desulfurization Liquors", M.S. Thesis, University of Arizona (1983)
12. Meserole, F. B., Personal Communication, Radian, Austin, 1983
13. Randolph, A. D. "CSD Dynamics, Stability, and Control" AICHE Symp. Ser., 76 (193), 1-5 (1980)
14. Randolph, A. D. and M. A. Larson "Theory of Particulate Processes", Academic Press, New York (1971)

15. Rase H. F., "Chemical Reactor Design for Process Plants; Principles and Techniques", 1, John Wiley & Sons, New York (1977)
16. Scheib, R. et al., J. Appl. Cryst., 7, 447-448 (1974)
17. Toprac, A. J. "Limestone Dissolution in Stack Gas Desulfurization Processes - Effect of Type and Grind", M.S. Thesis, University of Texas at Austin (1981)
18. Vaden, D. E. "Effects of Particle Size Classification on Gypsum Size Distribution in Simulated Stack Gas Scrubbing Liquors", M.S. Thesis, University of Arizona (1981)

Chapter 3

Dissolution Rate of Calcium Sulfite Hemihydrate in Flue Gas Desulfurization Processes

3.1 Summary

The rate of CaSO_3 dissolution in slurry scrubbers and hold tanks for flue gas desulfurization affects SO_2 absorption, limestone utilization and sulfite oxidation. The dissolution rates of CaSO_3 were measured by the pH-stat method. A mass transfer model was developed assuming that CaSO_3 particles behave as spheres in an infinite stagnant solution. The model combined with the Bechtel-modified Radian solution equilibrium program successfully predicts calcium sulfite dissolution rates at pH 3.5 - 5.5, 23 and 55 °C, 0.001 - 0.3 M Ca^{++} and 2 - 25 mM dissolved sulfite. The effects of sulfate content in solids and liquids and particle size/shape were also studied.

At conditions typical of flue gas desulfurization processes, CaSO_3 dissolution was controlled by mass transfer, not surface reaction kinetics. The rate of dissolution was a strong function of

pH, solution composition and temperature. Dissolution was fast at low pH and slowed near the equilibrium pH determined by dissolved Ca^{++} and $\text{SO}_3^{=}$ concentrations in the aqueous solutions, K_{sp} of the $\text{CaSO}_3 \cdot 1/2\text{H}_2\text{O}$ solids, and temperature. The presence of dissolved Mg^{++} increased the equilibrium pH and enhanced the dissolution rate. The presence of dissolved sulfate reduced the dissolution rate but did not change the equilibrium pH. The effect of sulfate was not adequately described by the mass transfer model.

3.2 Conclusions and Significance

1. The pH-stat method is effective in the measurement of calcium sulfite dissolution rates as a function of pH, temperature, and solution composition.
2. The dissolution of $\text{CaSO}_3 \cdot 1/2\text{H}_2\text{O}$ can be modelled successfully by stagnant mass transfer combined with the Bechtel-modified Radian solution equilibrium program. The dissolution rate is controlled by the diffusion of H^+ , $\text{SO}_3^{=}/\text{HSO}_3^-$ and CaSO_3^0 ion pairs, not by surface reaction kinetics.
3. The stagnant mass transfer model underpredicts the absolute dissolution rate by a factor of 1.7, probably because of the enhancement of the mass transfer coefficient due to the particle size/shape.

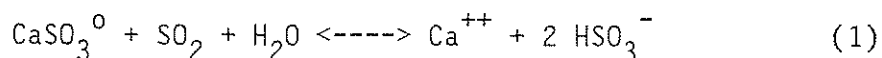
4. The solubility of $\text{CaSO}_3 \cdot 1/2\text{H}_2\text{O}$ is a function of temperature and the sulfate content in the solids. It decreases as the temperature increases and increases as the sulfate content in the solids increases.
5. Dissolved sulfate in the aqueous solution strongly inhibits $\text{CaSO}_3 \cdot 1/2\text{H}_2\text{O}$ dissolution, probably by surface adsorption.
6. Dissolved Mg^{++} enhances the rate of $\text{CaSO}_3 \cdot 1/2\text{H}_2\text{O}$ dissolution by forming strong ion pairs with $\text{SO}_3^{=}$.
7. The effects of temperature are predicted by the mass transfer model combined with the Stokes-Einstein equation for the ionic diffusivities and the corrected K_{sp} of $\text{CaSO}_3 \cdot 1/2\text{H}_2\text{O}$ as a function of temperature.

3.3 Introduction

The objective of this work is to measure and model the dissolution rate of calcium sulfite in flue gas desulfurization processes which absorb SO_2 by a slurry of lime or limestone with simultaneous calcium sulfite/sulfate crystallization. Calcium sulfite dissolution can be important in these processes because it affects the solution composition and chemical equilibria in the scrubbing solution, and therefore affects SO_2 absorption, sulfite

oxidation, and limestone dissolution (Chan and Rochelle, 1982). The rates of both SO_2 absorption and limestone dissolution are usually determined by mass transfer with equilibrium acid/base reactions in the solution (Rochelle and King, 1977; Chang and Rochelle, 1981; 1982; Weems, 1981; Sada, et al., 1983).

With low excess CaCO_3 or Ca(OH)_2 solids, as in low pH CaCO_3 scrubbing or general Ca(OH)_2 scrubbing processes, CaSO_3 will dissolve in the scrubber with the stoichiometry (Rochelle and King, 1977):



Intentional sulfite oxidation has been used to increase the SO_2 removal efficiency and to oxidize calcium sulfite ($\text{CaSO}_3 \cdot 1/2\text{H}_2\text{O}$) to gypsum ($\text{CaSO}_4 \cdot 2\text{H}_2\text{O}$) which generally consists of larger crystals, has less disposal volume and settles faster (Borgwardt, 1976; 1978). In forced oxidation of a bleed stream, or in a second-stage scrubber loop where $\text{CaSO}_3/\text{CaSO}_4$ has crystallized, sulfite oxidation kinetics can be limited by dissolved sulfite. Such operations require low pH to get CaSO_3 dissolution and subsequent oxidation. Erwin et al. (1981) and Nurmi et al. (1982) modeled the oxidation of calcium sulfite slurries in aqueous solutions and indicated that $\text{CaSO}_3 \cdot 1/2\text{H}_2\text{O}$ dissolution is controlled by mass transfer whereas sulfite oxidation is controlled by solution reaction kinetics.

The dissolution of ionic solids have been indicated to be

controlled either by surface kinetics or by diffusion of ions (Garside, et al., 1974; Plummer, et al., 1978; Chan and Rochelle, 1982; Meserole, et al., 1982). Chan (1981) measured CaCO_3 dissolution at flue gas desulfurization conditions using the pH-stat method, and modeled the experimental data by a stagnant mass transfer model with equilibrium acid/base reactions. That work was extended by Toprac and Rochelle (1982) who accounted for the dependence of dissolution rates on particle size and shape. Calcium sulfite dissolution is basically similar to calcite dissolution, but the solids composition is usually a mixture of $\text{CaSO}_3/\text{CaSO}_4$ instead of pure CaSO_3 and the particles can be aggregates of many small crystals. The shape of the crystals also varies from platelet to rosette. Jones et al. (1976) used X-ray, DSC, and IR to confirm the formation of a solid solution of calcium sulfate in $\text{CaSO}_3 \cdot 1/2\text{H}_2\text{O}$. Setoyama et al. (1978) found that the solubility of calcium sulfate in $\text{CaSO}_3 \cdot 1/2\text{H}_2\text{O}$ is a function of temperature.

The reported solubility (mg/l) of $\text{CaSO}_3 \cdot 1/2\text{H}_2\text{O}$ in water is 43 (18 °C, Weisberg, 1896), 46.3 (30 °C, van der Linden, 1917). Lowell et al. (1970) reports in the Radian solution equilibrium program a measured solubility of $\text{CaSO}_3 \cdot 1/2\text{H}_2\text{O}$ as the thermodynamic solubility product of $8.4 \times 10^{-8} \text{ M}^2$, and indicated that there is little change in solubility with temperature. Bechtel increased the K_{sp} to $4.498 \times 10^{-7} \text{ M}^2$ to match field data. Recently Faist et al. (1981) give an expression of $\text{CaSO}_3 \cdot 1/2\text{H}_2\text{O}$ solubility as a function of temperature:

$$\text{Log } K_{sp} = 838.3/T - 9.7572 \quad (2)$$

Discrepancies in these results may have resulted from the difficulties in controlling the dissolved sulfate concentration and the variation in solid sulfate content of the $\text{CaSO}_3 \cdot 1/2\text{H}_2\text{O}$ samples used in these experiments.

In this chapter, the dissolution rates of $\text{CaSO}_3 \cdot 1/2\text{H}_2\text{O}$ at conditions typical of flue gas desulfurization processes were measured by using the pH-stat method introduced by Chan (1981) and Prada (1981). A model was developed by using mass transfer with equilibrium acid/base reactions similar to Chan and Rochelle's work for CaCO_3 dissolution (1982). This work is a part of an effort for overall scrubber modeling which includes rate models for SO_2 absorption, CaCO_3 dissolution, sulfite oxidation, and CaSO_3 dissolution and crystallization (Mehta, 1982; Chan and Rochelle, 1983).

The CaSO_3 dissolution experiments were conducted at pH 3.5 - 6, 0.001 - 0.3 M Ca^{++} , 1 - 10 mM dissolved sulfite, 23 and 55 °C, 0.3 - 0.9 eq/l ionic strength, and 0 - 200% gypsum saturation. Three batches of CaSO_3 seed crystals were used to study the effects of particle size and shape. The effects of pH, sulfite, sulfate, temperature and ionic strength were investigated and the solubility product of $\text{CaSO}_3 \cdot 1/2\text{H}_2\text{O}$ were found to be a function of temperature and the sulfate content in the solids.

3.4 Theory

Limestone and calcium sulfite dissolution can both be modeled as steady-state mass transfer between the solid surface and the bulk solution (Chan and Rochelle, 1982; Erwin, et al., 1982; Mehta and Rochelle, 1983). A steady-state solution of the mass transfer model is obtained by assuming spherical CaSO_3 particles in an infinite stagnant solution, corresponding to a mass transfer coefficient equal to the ratio of diffusivity to particle radius (D/r).

3.4.1 Effect of Solution Composition

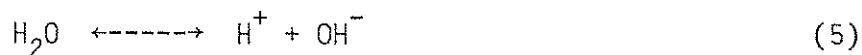
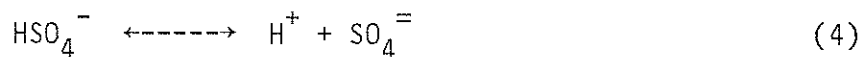
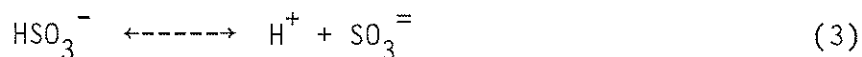
The main feature of the mass transfer model is that chemical equilibrium is maintained throughout the diffusion path for all chemical species. As shown in Figure 3-1, H^+ diffuses through the boundary layer from bulk solution to calcium sulfite particle surface and the dissolved $\text{SO}_3^{=}/\text{HSO}_3^-$ or CaSO_3^0 diffuses from sulfite particle surface to bulk solution. The boundary condition at the particle surface is assumed to be governed by the CaSO_3 solubility product, and that at the bulk solution be governed by the specified pH (operating pH). Chemical equilibria, ionic electroneutrality, and material balances are then used to determine the concentrations of all chemical and ionic species in the boundary layer.

This model utilizes pseudo-equilibrium constants derived from the Bechtel-modified Radian solution equilibrium program, so that the

equilibrium program needs to be called only once during the calcium sulfite dissolution modeling work. The effects of ion pairs are accounted for by the pseudo-equilibrium constants, and there are no direct ion pair equilibria. Therefore, solution of the mass diffusion equations is greatly simplified.

(i) Solution Equilibria

In this work, the important solution equilibria for CaSO_3 dissolution were:



Additional equilibria would need to be added to simulate the effects of other buffers such as organic acids and $\text{CO}_2/\text{HCO}_3^-$.

Using the Bechtel-modified Radian equilibrium program, the concentrations of various chemical species were calculated. In order to perform the mass transfer calculation without manipulating ion pair equilibria, the following pseudo-concentrations were defined:

(ii) Pseudo-Concentrations

$$[\text{Ca}^{++}]' = [\text{Ca}^{++}] + [\text{CaOH}^+] + [\text{CaSO}_3^0] + [\text{CaSO}_4^0] \quad (6)$$

$$[\text{SO}_3^=]' = [\text{SO}_3^=] + [\text{CaSO}_3^0] + [\text{MgSO}_3^0] \quad (7)$$

$$[\text{SO}_4^=]' = [\text{SO}_4^=] + [\text{CaSO}_4^0] + [\text{MgSO}_4^0] + [\text{NaSO}_4^-] \quad (8)$$

$$[\text{OH}^-]' = [\text{OH}^-] + [\text{CaOH}^-] + [\text{MgOH}^-] \quad (9)$$

The pseudo-concentrations for HSO_3^- , HSO_4^- , and H^+ are equal to their true concentrations due to the absence or the insignificance of ion pairs including these species.

(iii) Diffusion Coefficients:

Values of diffusion coefficients used in the model are given in Table 3-1 (Chan and Rochelle, 1982). At 25°C and infinite dilution, ionic diffusivities were calculated by:

$$D = RT\lambda_o / n_j(Fa)^2 \quad (10)$$

where Fa is the Faraday number, n_j is the charge on the j_{th} ion, and λ_o is the equivalent ionic conductivity.

Diffusivities at 55°C were estimated by the Stokes-Einstein relationship:

$$D_1\eta_1 / T_1 = D_2\eta_2 / T_2 \quad (11)$$

Table 3-1: Diffusivities at 25 °C

Species	$D \times 10^{-5} \text{ (cm}^2\text{/sec)}$
HSO_4^-	1.33
$\text{SO}_4^{=}$	1.06
HSO_3^-	1.33
$\text{SO}_3^{=}$	0.96
Ca^{++}	0.79
H^+	9.31
OH^-	5.27
CaSO_3^0	0.53
MgSO_3^0	0.53

(iv) Pseudo-diffusivities:

To use the pseudo-concentrations in the solution equilibrium program, pseudo-diffusivities have been defined for all the pseudo chemical species defined above:

$$D_j^i = (\sum D_i C_i) / \sum C_i \quad (12)$$

which is summed over all species i containing component j . For example, to calculate the pseudo-diffusivity for the pseudo-species, Ca^{++} , let $j = \text{Ca}^{++}$ and $i = \text{Ca}^{++}, \text{CaOH}^+, \text{CaSO}_3^0, \text{CaSO}_4^0$. The pseudo-diffusivities for HSO_3^- , HSO_4^- , and H^+ are set equal to their true diffusivities.

(v) Pseudo-equilibrium constants:

Based on the above pseudo-concentrations, the pseudo-equilibrium constants were calculated as follows:

$$K_w = [H^+] [OH^-]' \quad (13)$$

$$K_{HSO_4^-} = ([H^+] [SO_4^{2-}]') / [HSO_4^-] \quad (14)$$

$$K_{HSO_3^-} = ([H^+] [SO_3^{2-}]') / [HSO_3^-] \quad (15)$$

$$SK_{sp} = (K_{sp} [Ca^{+2}]' [SO_3^{2-}]') / ([Ca^{+2}] [SO_3^{2-}]) \quad (16)$$

(vi) Diffusion Balances:

In general the flux of a component is given by:

$$\text{Flux}_j = D_j ([J_j]_i - [J_j]_b) / \delta \quad (17)$$

The calcium sulfite dissolution flux is defined as the sum of sulfite flux and bisulfite flux:

$$\begin{aligned} \text{Dissolution Flux} &= D_{SO_3^{2-}}' ([SO_3^{2-}]_i' - [SO_3^{2-}]_b') / \delta \\ &+ D_{HSO_3^-} ([HSO_3^-]_i - [HSO_3^-]_b) / \delta \quad (18) \end{aligned}$$

where the subscripts i and b denote solid-liquid interface and bulk solution respectively, and δ is the boundary layer thickness.

By the principle of electroneutrality, the net flux of electric charge in the boundary layer is equal to zero:

$$\begin{aligned}
 2 \text{ Ca}^{++} \text{ flux} + \text{ H}^+ \text{ flux} - 2 \text{ SO}_3^- \text{ flux} - 2 \text{ SO}_4^- \text{ flux} \\
 - \text{ HSO}_3^- \text{ flux} - \text{ HSO}_4^- \text{ flux} - \text{ OH}^- \text{ flux} = 0
 \end{aligned} \quad (19)$$

By stoichiometry the calcium flux must be equal to the total flux of sulfite and sulfate from the solid:

$$\begin{aligned}
 \text{ Ca}^{++} \text{ flux} = \text{ SO}_3^- \text{ flux} + \text{ HSO}_3^- \text{ flux} + \text{ SO}_4^- \text{ flux} \\
 + \text{ HSO}_4^- \text{ flux}
 \end{aligned} \quad (20)$$

By stoichiometry the ratio of the fluxes of total sulfite and total sulfate must be the same as the composition of the solid:

$$\begin{aligned}
 (\text{ SO}_3^- \text{ flux} + \text{ HSO}_3^- \text{ flux}) / (1 - Y_{\text{SO}_4}) \\
 = (\text{ SO}_4^- \text{ flux} + \text{ HSO}_4^- \text{ flux}) / Y_{\text{SO}_4}
 \end{aligned} \quad (21)$$

where Y_{SO_4} is the mole fraction of sulfate in the calcium sulfite solids.

(vii) Solution of the surface diffusion balances and equilibria:

In the mass transfer model, there are eight unknowns in the solution boundary layer surrounding the CaSO_3 particle: $[\text{Ca}^{++}]'$, $[\text{SO}_3^-]'$, $[\text{SO}_4^-]'$, $[\text{OH}^-]'$, $[\text{HSO}_4^-]$, $[\text{HSO}_3^-]$, $[\text{H}^+]$, and the CaSO_3 ,

dissolution flux. Material and charge balances (Equations 18 to 21) and chemical equilibria (Equations 13 to 15) were solved by iteration on pH at the particle surface. Bulk pH was used as an initial guess. The boundary condition from solubility was used to check for convergence:

$$\text{B.C.} \quad [\text{Ca}^{+}]' [\text{SO}_3^=]' = SK_{\text{sp}} \quad (22)$$

The product of the calculated pseudo-concentrations of Ca^{++} and $\text{SO}_3^=$ at the particle surface was compared with the boundary condition. The guessed surface H^+ concentration was then reduced by a factor of 2 each time until the difference changed sign. After bracketing the H^+ concentration, a half-interval method was used to find the surface H^+ concentration that satisfied the boundary condition. Equation 18 was then used to calculate the product of boundary layer thickness and CaSO_3 dissolution flux. This quantity (DAC) is used in the next section to give an effective product of the diffusion coefficient and driving force.

3.4.2 Effect of Particle Size Distribution

The rate of dissolution of a single spherical particle can be represented by the proportionality (Chan and Rochelle, 1981):

$$-dV/dt = Sh \pi d_p (DAC) / \rho_m \quad (23)$$

where $Sh = k_c d_p / D$. For small spherical particles in stagnant solution, assuming Sh is independent of d_p and is approximately equal to 2 (Toprac, 1981), integrating the above equation gives:

$$f = \text{fraction remaining} = V/V_o = (1 - kt/d_p^2)^{1.5} \quad (24)$$

where $k = 4 Sh D \Delta C / \rho_m \approx 8 D \Delta C / \rho_m$. The molecular weight of calcium sulfite was taken as 129.0 gram/mole, which was calculated from the molecular formula of $CaSO_3 \cdot 1/2 H_2O$. The molar density of calcium sulfite hemihydrate was taken to be 0.0194 gmol/cm³.

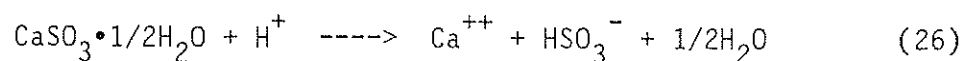
For polydisperse solids, the total fraction remaining, F , can be determined by summing over the differential size distribution ϕ where ϕ_j is the fraction of total particle volume with diameters from d_j to d_{j+1} :

$$F = V/V_o = \sum \phi_j (1 - kt/d_j d_{j+1})^{1.5} \quad (25)$$

3.5 Experimental

3.5.1 Dissolution Rate Measurement

The calcium sulfite dissolution rate was determined by the pH-stat method in an agitated, stirred tank reactor (Figure 3-2). The pH-stat apparatus (Figure 3-3) was the same as that used previously for measurement of CaCO_3 dissolution (Chan and Rochelle, 1982) and sulfite oxidation (Ulrich et al., 1984). The agitator speed was set at 720 rpm. The reactor was sparged with N_2 before adding the CaSO_3 solids and was blanketed with N_2 during the rate measurement. The pH was automatically controlled to ± 0.02 units by titrating with 0.04 to 0.2 N HCl. Calcium sulfite dissolution rate was related to the titration rate by the stoichiometry:



The dissolution rate at high pH was corrected by a calibration of the $\text{SO}_3^{=}/\text{HSO}_3^-$ equilibrium.

The compositions of the aqueous solution simulate the operating conditions of actual scrubber systems. Two mmoles of $\text{CaSO}_3 \cdot 1/2\text{H}_2\text{O}$ solids were put in one liter of solution at the beginning of each dissolution experiment. CaSO_3 sample 1 was used in most of the dissolution experiments, samples 3 and 5 were also used in some experimental runs to study the effect of solids variation.

During a batch experiment the pH was constant, and both Ca^{++} and total dissolved sulfite concentration increased slightly. After the addition of Na_2SO_3 , the gas dispersion tube was lifted to avoid stripping of SO_2 . Most of the experiments were performed at room temperature, but some runs were at 55 °C to study the effect of temperature.

3.5.2 Synthesis and Characterization of Calcium Sulfite Samples

Three batches of $\text{CaSO}_3 \cdot 1/2\text{H}_2\text{O}$ samples were synthesized in the laboratory by reacting solutions of CaCl_2 with $\text{Na}_2\text{SO}_3/\text{Na}_2\text{SO}_4$. The solids were characterized by iodometric titration, differential scanning calorimetry, X-ray powder diffraction, infrared spectroscopy, scanning electron microscopy, BET surface area measurement, and particle size analysis (Coulter Counter). The results are listed in Table 2-1 and are discussed in detail in Chapter 2.

3.5.3 Experimental rate constant determination

A typical dissolution experiment is shown in Figure 3-4. The total fraction remaining, F , calculated from the volume of HCl added is given as a function of dimensionless time, t/t_{50} , where t_{50} is the time required to dissolve 50% of the $\text{CaSO}_3 \cdot 1/2\text{H}_2\text{O}$ solids. A calculated curve is also given using the stagnant mass transfer model incorporated with the polydisperse particle size distribution. As

shown in Figure 3-4, the shape of the polydisperse stagnant mass transfer model fits the experimental data very well.

The experimental rate constant, k , was determined by using Equation 24 with the calculated and measured values of F at kt_{55} and kt_{45} . For the typical experimental run at pH 4.3, $t_{55} = 10.1$ minutes, $t_{45} = 7.35$ minutes. From Equation 26 and the initial CaSO_3 particle size distribution, the calculated $kt_{55} = 160.6 \times 10^{-8} \text{ cm}^2$, and $kt_{45} = 112.3 \times 10^{-8} \text{ cm}^2$. Therefore,

$$\begin{aligned} k &= (kt_{55} - kt_{45}) / (t_{55} - t_{45}) \\ &= 2.93 \times 10^{-9} \text{ cm}^2/\text{sec} \end{aligned} \quad (27)$$

3.6 Results and Discussion

The $\text{CaSO}_3 \cdot 1/2\text{H}_2\text{O}$ dissolution rates were measured with various solution compositions, ionic strength, temperature, gypsum saturation and seed crystals. The mass transfer model accurately predicts the effects of all variables except for inhibition by the dissolved sulfate.

The curves given in figures 3-5 through 3-10 were calculated by the mass transfer model with adjustment of the Sherwood number and K_{sp} for each seed crystal (Table 3-2). The observed values of Sh (3.4 to 4.0) are expected with the particle size and shape observed.

There is no evidence of any effect of surface kinetics, even at conditions near equilibrium pH, except in the presence of dissolved sulfate.

3.6.1 Effect of Particle Size/Shape and Sulfate Content in Solids

Three batches of CaSO_3 samples with different sulfate content and particle size/shape were used in a series of dissolution experiments. As shown in Figure 3-5, the experimental data were best represented using a Sherwood number of 3.4 with seed 1, 3.8 with seed 3, and 4.0 with seed 5. The stagnant mass transfer model with a Sherwood number of 2 underpredicted the dissolution rates due to the deviation of the CaSO_3 particle size/shape from small diameter and smooth spheres. Values of the Sherwood number calculated from Toprac's (1982) correlation with limestone particles using average particle sizes are 3.42, 2.78 and 3.61 respectively. Solids with lower CaSO_4 content tend to have lower dissolution rates with decreased equilibrium pH. The experimental data were best represented by letting K_{sp} vary with sulfate content (Table 3-2). The deduced values of K_{sp} are between those used by Bechtel (Epstein, 1975) and Radian (Lowell, et al., 1970).

Table 3-2: Adjusted Sh and K_{sp} of $\text{CaSO}_3 \cdot 1/2\text{H}_2\text{O}$ as a Function of Solid Sulfate Content and Temperature

CaSO_3 Seed Crystal	Sample 1	Sample 2	Sample 3
Mole % CaSO_4	5.1	10.6	3.0
K_{sp} at 23 °C (M^2)	2.67×10^{-7}	3.40×10^{-7}	2.40×10^{-7}
K_{sp} at 55 °C (M^2)	1.12×10^{-7}	1.44×10^{-7}	1.01×10^{-7}
Sherwood No.	3.4	3.8	4.0

3.6.2 Effect of temperature

Higher temperature affects $\text{CaSO}_3 \cdot 1/2\text{H}_2\text{O}$ dissolution rate by increasing diffusion coefficients and reducing $\text{CaSO}_3 \cdot 1/2\text{H}_2\text{O}$ solubility (K_{sp}). Figure 3-6 shows that at low pH, mass transfer is important and CaSO_3 dissolves faster because of higher diffusivities. At high pH, chemical equilibrium is important and the effect of the solubility product dominates, so that CaSO_3 has a lower dissolution rate. The value of K_{sp} at 55 °C for seed 1 was implied to be only 42% of that at 23 °C, corresponding to a heat of solution of -2.6 kcal/gmol (Table 3-2).

3.6.3 Effect of pH and Dissolved Sulfite

The effects of pH and total dissolved sulfite (S^{+4}) on calcium sulfite dissolution rate are shown in Figure 3-7. At low pH, the pH has a strong and almost linear effect on dissolution rate, suggesting that H^+ diffusion determines the dissolution rate of calcium sulfite. At high pH, however, the dissolved sulfite is significant because chemical equilibrium becomes important. The mass transfer model with adjusted K_{sp} values predicts the dissolution rates very well.

3.6.4 Effect of Dissolved Sulfate

The presence of sulfate in the aqueous solution reduces the $CaSO_3$ dissolution rate. Figure 3-8 is a plot of the experimental rate constant k versus sulfate concentration at pH 4.2, in a solution of 0.1 M $CaCl_2$ and 10 mM S^{+4} . It shows that the presence of dissolved sulfate strongly inhibits the calcium sulfite dissolution rate.

In terms of the mass transfer model, dissolved sulfate appears to reduce the Sherwood number (Figure 3-8). Dissolved sulfate could shift Sh by essentially stopping dissolution on certain crystal faces without affecting dissolution of the other faces. So that the effective area is reduced, but the dissolution rate is still controlled by mass transfer.

Figure 3-9 represents the experimental rate constant k as a function of pH and dissolved sulfate concentration. The presence of dissolved sulfate reduced calcium sulfite dissolution rate at both high pH and low pH. As shown previously in Figure 3-6, the presence of dissolved sulfate at high temperature reduces CaSO_3 dissolution rate in the same manner as it does at room temperature. So that the role of sulfate in CaSO_3 dissolution is not strongly affected by the temperature change.

3.6.5 Effect of Ionic Environment and Ca^{++} Concentration

As shown in Figure 3-10, the dissolution rate of calcium sulfite was measured in five different solution compositions of the same ionic strength (0.3 eq/l). Ca^{++} has a strong effect on dissolution rate and equilibrium pH because $[\text{Ca}^{++}]$ directly determines the solubility product of calcium sulfite in the aqueous solution. However, dissolved Mg^{++} makes $\text{CaSO}_3 \cdot 1/2\text{H}_2\text{O}$ dissolve faster because it forms an ion pair with $\text{SO}_3^{=}$. The mass transfer model accounts for this effect. The agreement of experimental and calculated results indicates that Mg^{++} does not have additional effects on CaSO_3 dissolution, such as reducing the rate of surface reaction by adsorption.

In Figure 3-11, the $\text{CaSO}_3 \cdot 1/2\text{H}_2\text{O}$ dissolution rates were measured at a higher ionic strength (0.9 eq/l). The same effects of the dissolved Ca^{++} and Mg^{++} were observed. The mass transfer model

predicts the dissolution rates fairly well but the deviation of Mg^{++} data suggests that some correction or modification of the diffusivities or equilibrium constants in the solution equilibrium program may be necessary at higher ionic strength.

3.7 Nomenclature

C	concentration	(M)
D	diffusivity	(cm^2/sec)
D'	pseudo-diffusivity	(cm^2/sec)
Fa	Faraday constant	= 23,062 (cal/volt-equiv)
K	equilibrium constant	
K _{sp}	solubility product	(M^2)
M	molarity	(gmol/liter)
R	gas constant	= 1.987 (cal/gmol-°K)
Sh	Sherwood number	($k_c d_p / D$)
SK _{sp}	pseudo-solubility product	(M^2)
T	temperature	(°K)
V	volume of particle	(cm^3)
Y _{SO₄}	mole fraction of sulfate content	
a	activity	(M)
d _p	particle diameter	(cm)
k	rate constant	(cm^2/sec)
k _c	mass transfer coefficient	(cm/sec)
r	radius	(cm)
t	time	(sec)
λ _o	equivalent ionic conductivity at infinite dilution	($\text{cm}^2/\text{gmole-ohm}$)
η	viscosity	(poise)
ρ	density	(gram/cm ³)

ρ_m	molar density	(gmol/cm ³)
ϕ	volume fraction	
[]	concentration	(M)
[]'	pseudo-concentration	(M)

Superscripts

+	positive charge
-	negative charge
o	ion pair, degrees

Subscripts

b	bulk solution
i	solid-liquid interface
o	initial state

3.8 Literature Cited

1. Borgwardt, R. H., "Proceedings: Symposium on Flue Gas Desulfurization", EPA-600/2-76-136a, 117 - 144 (1976)
2. Borgwardt, R. H., "Proceedings: Symposium on Flue Gas Desulfurization", EPA-600/7-78-058a, 205 - 208 (1978)
3. Chan, P. K. "CaCO₃ Dissolution in SO₂ Scrubbing Solution, Mass Transfer Enhanced by Chemical Reactions.", M.S. Thesis, University of Texas at Austin (1981)
4. Chan, P. K. and G. T. Rochelle, "Limestone Dissolution: Effects of pH, CO₂, and Buffers Modeled by Mass Transfer", ACS Symp. Ser., 188, 75-97 (1982)
5. Chan, P. K. and G. T. Rochelle, "Modeling of SO₂ Removal by Limestone Slurry Scrubbing: Effects of Chlorides", Presented at EPA/EPRI Symposium on Flue Gas Desulfurization, New Orleans, November 1-4, 1983
6. Chang, C. S. and G. T. Rochelle, "Mass Transfer Enhanced by Equilibrium Reactions." Ind. Eng. Chem. Fundam., 21, 379-385 (1982)
7. Chang, C. S. and G. T. Rochelle, "SO₂ Absorption Into Aqueous Solutions." AIChE J., 27, 292-298 (1981)

8. Chang, C.S. and G.T. Rochelle, "Effect of Organic Acid Additives on SO_2 Absorption into CaO/CaCO_3 Slurries." AIChE J., 28, 261-266 (1982)
9. Epstein, M., "EPA Alkali Scrubbing Test Facility: Summary of Testing Through October 1974", EPA-650/2-75-047 (1975)
10. Erwin, J., Wang, C. C. and J. L. Hudson, "A model of Oxidation in Calcium Sulfite Slurries." ACS Symp. Ser., 188, 191-220 (1982)
11. Faist, M. B., Riese, C. E. and L. Gevirtzman, "Species Distribution Model: A General Computer Program to Calculate The Distribution of Chemical Species Among Several Multicomponent Phases", DOE Contract No. DE-AC21-80MC14549, Radian (1981)
12. Garside, J., Mullin J. W. and S.N. Das, "Growth and Dissolution Kinetics of Potassium Sulfate Crystals in an Agitated Vessel." Ind. Eng. Chem. Fundam., 13, 299-305 (1974)
13. Jones, B.F., Lowell, P. S. and F.B. Meserole "Experimental and Theoretical Studies of Solid Solution Formation in Lime and Limestone SO_2 Scrubbers." EPA-600/2-76-273a (1976)

14. Linden, T. van der., J. Soc. Chem. Ind., 36, 96 (1917)
15. Lowell, P. S., Ottmers, D. M., Strange, T. I., Schwitzgebel, K., and D. W. DeBerry, "A Theoretical Description of The Limestone Injection - Wet Scrubbing Process", Radian, Contract No. CPA-22-69-138 v(1970)
16. Mehta, R.R. "Modeling of SO₂ Removal and Limestone Utilization in Slurry Scrubbing with Forced Oxidation", M.S. Thesis, University of Texas at Austin (1982)
17. Meserole, F.B., Glover, R.L. and D.A. Stewart, "Studies of the Major Factors Affecting Magnesium Limestone Dissolution", ACS Symp. Ser., 188, 99-111 (1982)
18. Nurmi, D. B., Overman, J. W., Erwin, J. and J. L. Hudson, "Sulfite Oxidation in Organic Acid Solutions", ACS Symp. Ser., 188, 173 - 189 (1982)
19. Plummer, L. N., Wigley, T. M. L., and D. L. Parkhurst "The Kinetics of Calcite Dissolution in CO₂-Water Systems", Am. J. Sci., 278, 179-216 (1978)
20. Rochelle, G.T. and C.J. King "The Effect of Additives on Mass Transfer in CaO/CaCO₃ Slurry Scrubbing of SO₂ From Waste Gases." Ind. Eng. Chem. Fundam., 16, 67-75 (1977)

21. Sada, E., Kumazawa, H., and M. A. Butt, "Absorption of Sulfur Dioxide into Aqueous Slurries of Sparingly Soluble Fine Particles" Chem. Eng. Sci., 35, 771-777 (1980)
22. Sada, E., Kumazawa, H., and H. Nishimura "Absorption of Sulfur Dioxide into Aqueous Double Slurries Containing Limestone and Magnesium Hydroxide", AIChE J., 29, 60-65 (1983)
23. Setoyama, K. and S. Takahashi, "Solid Solution of Calcium Sulfite Hemihydrate and Calcium Sulfate", Yogyo-Kyokai-Shi, 86, 56 - 62 (1978)
24. Toprac, A. J., M. S. Thesis, University of Texas, Austin, Texas (1981)
25. Toprac, A.J. "Limestone Dissolution in Stack Gas Desulfurization", Environ. Prog., 1, 52 - 58 (1982)
26. Ulrich, R. K., Rochelle, G. T., and R. E. Prada, "Enhanced Oxygen Absorption Into Bisulfite Solutions Containing Transition Metal Ion Catalysts", Submitted to Chem. Eng. Sci., (1984)
27. Weems, W.T. "Enhanced Absorption of SO₂ by Sulfite and

Other Buffers." M.S. Thesis, University of Texas at Austin
(1981)

28. Weisberg, J., B1. Soc. Chim., 3, (15) 1247 - 1250 (1896)

Chapter 4

CaSO₃ Crystal Growth Rate and Crystal Habit

4.1 Summary

The crystal growth rate of CaSO₃•1/2H₂O was measured by a pH-stat method in aqueous solution with pH 3.5 to 6.5, 1 to 25 mM dissolved sulfite, 0.01 to 0.3 M Ca⁺⁺, and 0 to 25 mM sulfate. The growth rate was a strong function of relative supersaturation and was strongly inhibited by dissolved sulfate. The growth rate per unit BET surface area, R^i (mole/cm²-min), is given by: $9.7 \times 10^{-4} \exp(-10250/RT) \times (RS_{CaSO_3} - 1)^2 \times RS_{CaSO_4}^{-1}$, where RS_{CaSO_3} and RS_{CaSO_4} are the relative saturations with respect to calcium sulfite and gypsum, respectively. Scanning electron microscopy and IR spectroscopy demonstrated that solids generated in the presence of dissolved sulfate contained solid solution sulfate and crystallized as agglomerates of very thin platelets. In the absence of solid or dissolved sulfate the solids were agglomerates of well-formed columnar, hexagonal crystals.

4.2 Conclusions and Significance

1. The crystal growth of $\text{CaSO}_3 \cdot 1/2\text{H}_2\text{O}$ is controlled by surface kinetics, not by diffusion in a solution boundary layer.
2. The crystal growth rate is second order in $\text{CaSO}_3 \cdot 1/2\text{H}_2\text{O}$ supersaturation, and the estimated activation energy is 10 kcal/gmole.
3. Dissolved sulfate strongly inhibits the crystal growth of $\text{CaSO}_3 \cdot 1/2\text{H}_2\text{O}$. The rate of crystal growth is inversely proportional to the gypsum saturation.
4. Dissolved sulfate changes the crystal habit from columnar to platelet. The dewatering properties of waste solids from flue gas desulfurization processes should be enhanced by inhibiting sulfite oxidation.
5. Crystal habit mainly depends on solution composition and temperature. Seed crystal variation has no significant effect on the ultimate crystal habit.

4.3 Introduction

The crystallization of calcium sulfite hemihydrate is of importance in flue gas desulfurization processes which absorb SO_2 by a slurry of lime or limestone with simultaneous calcium sulfite/sulfate precipitation. Calcium sulfite crystallization affects the composition and chemical equilibria in the scrubbing solution, and therefore affects SO_2 absorption and limestone dissolution which are mass transfer controlled phenomena enhanced by equilibrium reactions (Rochelle and King, 1977; Chang and Rochelle, 1981, 1982; Chan and Rochelle, 1982; Sada et al., 1983). The habit of the grown calcium sulfite crystals is of particular interest because it determines the ease of dewatering, and thus affects the operation of solid-liquid separation processes (Borgwardt, 1976). Recently, limestone has been substituted for lime in dual-alkali processes (Glancy, et al., 1983; Chang and Kaplan, 1983); the crystallization rate and crystal habit of calcium sulfite are critical to the development of this next generation of technologies.

The earliest study of $\text{CaSO}_3 \cdot 1/2\text{H}_2\text{O}$ crystallization rate was conducted by Ottmers, et al. (1974). A continuous-liquid/batch-solid method was used and the crystallization rate was found to be first order relative to supersaturation. Nucleation was not significant when the relative supersaturation was below 3 or 4, and dominated above this level of supersaturation.

The ease of solids dewatering is strongly related to crystal size. Phillips et al. (1978) developed a mathematical model to relate calcium sulfite crystal size distribution to FGD operating conditions. Discrepancies in crystal size measurement in the micrometer range by using different methods were investigated by Edwards, et al. (1979). The results confirmed the reliability of measurement by a Coulter Counter, which has been extensively used in recent crystal size studies (Chan and Rochelle, 1982; Toprac and Rochelle, 1983; Etherton and Randolph, 1981; Erwin, et al., 1981; Kelly, et al., 1983).

Since the flue gas is usually accompanied by air, some sulfite is oxidized to sulfate and a mixture of calcium sulfite/sulfate crystallization product is usually obtained. Jones, et al. (1976) used X-ray, Differential Scanning Calorimetry and Infrared Spectroscopy to confirm the formation of a solid solution of calcium sulfate in calcium sulfite hemihydrate. It was indicated that the coprecipitation of sulfate with calcium sulfite hemihydrate is basically an equilibrium controlled process. Setoyama et al. (1978) found that the solubility of calcium sulfate in calcium sulfite hemihydrate is a function of reaction temperature. The calcium sulfate substituted up to about 9 mol% to form solid solution with little changes in lattice parameters from X-ray diffraction, but calcium sulfate content greater than 9 mol% caused disorder of the calcium sulfite crystal.

Crystal habit is another important factor which determines the quality of the crystallization product. Kelly and Randolph (1983) studied the effects of several crystal habit modifiers, mostly organic acids, on the size and morphology of calcium sulfite hemihydrate crystals. It was found that the presence of citric acid significantly reduces crystal growth rate and particle size, and produces spiny crystals; nitrilotris methylene triphosphoric acid (NMTP) on the other hand produces disc crystals. Meserole et al. (1983) found that calcium sulfite precipitation kinetics are not affected by high chloride concentrations but can be enhanced by high concentrations of dissolved sulfate. Solution composition was found to influence the calcium sulfite crystal size and habit. Calcium sulfite precipitated in the presence of high sulfate concentration was rod shaped or globular with some foliated growth patterns, whereas that precipitated in the presence of high chloride concentration or in dilute solutions was lamellar or acicular in habit.

A number of results from industrial development strongly suggest that gypsum saturation affects dewatering properties and crystal habit of CaSO_3 . In experiments simulating the hold tank of a CaCO_3 slurry scrubber, M. W. Kellogg found that large, easily dewatered CaSO_3 crystals were formed in the absence of sulfate (Cares, 1982). Development of the limestone dual alkali process has shown that dewatering of the calcium sulfite solids is difficult at

low ratios of dissolved sulfite to sulfate, but easy at high ratios (Chang and Kaplan, 1983). Previous work has shown that low dissolved sulfite/sulfate ratios give solutions with higher gypsum saturation and higher sulfate content in the solids (LaMantia et al., 1974). Recent work using sodium thiosulfate as an oxidation inhibitor has shown that adequate levels of thiosulfate enhance dewatering of the calcium sulfite solids, probably because of the significantly reduced gypsum saturation (Wang, 1982; Barkley et al., 1983; Acurex, 1984).

In this chapter, an expression of $\text{CaSO}_3 \cdot 1/2\text{H}_2\text{O}$ crystal growth kinetics was obtained and the crystal habit was studied at conditions typical of flue gas desulfurization processes. The crystallization experiments were conducted at pH 3.5 - 6.5, with most runs at room temperature and some at 55 °C. Relative supersaturations were 1.5 to 7. Typical scrubbing solution composition was varied from 0.01 to 0.3 M Ca^{++} , 0.2 to 0.9 M Cl^- , 1 to 25 mM total sulfite (S^{+4}), 0.3 to 0.9 eq/l ionic strength, and 0 to 250 % gypsum saturation. The calcium sulfite seed crystals used in the experiments had different crystal morphology and sizes, and were agglomerates rather than single crystals.

4.4 Experimental

4.4.1 Seed Crystal Synthesis and Characterization

Three batches of calcium sulfite seed crystals were synthesized in the laboratory by reacting solutions of calcium chloride and sodium sulfite/sodium sulfate. The solids were characterized (Table 4-1) by iodometric titration, differential scanning calorimetry, X-ray powder diffraction, infrared spectroscopy, scanning electron microscopy, BET surface area measurement, and particle size analysis by Coulter Counter. This work is discussed in detail in Chapter 2.

4.4.2 Crystal Growth Rate Measurement

Measurement of calcium sulfite crystal growth rates was performed in a batch stirred-tank reactor using the pH-stat method. The pH-stat apparatus was the same as that used previously for measurement of CaCO_3 dissolution (Chan and Rochelle, 1982) and sulfite oxidation (Ulrich et al., 1983). The agitator speed was set at 480 rpm. The reactor was sparged with N_2 before adding the seed crystals and was blanketed with N_2 during the rate experiment. The pH was automatically controlled to ± 0.02 units by titrating with 0.2 M Na_2SO_3 . Calcium sulfite crystal growth rate was related to the titration rate by the stoichiometry:

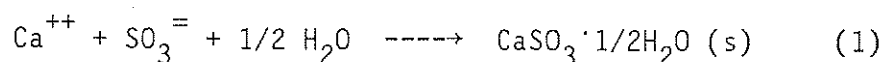


Table 4-1: CaSO_3 Seed Crystals

Sample No.	1	3	5
Mole % CaSO_4 by iodometric titration	5.1	10.6	3.0
Mole % CaSO_4 by infrared spectroscopy	3.4	10.7	1.0
Particle size (μm)	22 ± 10	12 ± 10	25 ± 10
Crystal habit	Platelet	Thin platelet	Columnar, hexagonal
Platelet thickness (μm)	0.1	0.01	2
BET surface area (m^2/gram)	1.92	9.54	1.23

Table 4-2: Corrected Values of K_{sp} of $\text{CaSO}_3 \cdot 1/2\text{H}_2\text{O}$ as
a Function of Temperature and Solid Sulfate Content

Seed Crystal	1	3	5
Mole % CaSO_4	5.1	10.6	3.0
K_{sp} at 23 °C (M^2)	2.67×10^{-7}	3.40×10^{-7}	2.40×10^{-7}
K_{sp} at 55 °C (M^2)	1.12×10^{-7}	1.44×10^{-7}	1.01×10^{-7}

* K_{sp} is defined as the product of Ca^{++} and $\text{SO}_3^{=}$ activities

The activities of Ca^{++} and $\text{SO}_3^{=}$ are strong functions of ionic equilibria. Supersaturations were calculated by the Bechtel-modified Radian solution equilibrium program (Lowell et al., 1970). The calcium sulfite relative saturation, $\text{RS}_{\text{CaSO}_3}$, is defined as:

$$\text{RS}_{\text{CaSO}_3} = (a_{\text{Ca}^{++}} a_{\text{SO}_3^{=}}) / K_{sp} \text{ of } \text{CaSO}_3 \cdot 1/2\text{H}_2\text{O} \quad (2)$$

Corrected values of the $\text{CaSO}_3 \cdot 1/2\text{H}_2\text{O}$ solubility product (Table 4-2) were used based on previous work on calcium sulfite dissolution (Chapter 3).

One mmole/liter seed crystal was put in the reactor at the beginning of each crystallization experiment, and was allowed to grow

to 4 - 8 mmole/liter. Seed 1 (Figure 2-8) was used in most of the crystallization experiments, seeds 3 and 5 (Figures 2-10 and 2-12) were also used in some experimental runs to study the effect of seed crystal variation. During a batch experiment the pH and total dissolved sulfite were constant, but Ca^{++} concentration decreased slightly. The gas dispersion tube was lifted to allow sparging N_2 above the liquid level after the addition of Na_2SO_3 to the solution to avoid stripping of SO_2 . Most of the experiments were performed at room temperature, but some runs were made at 55 °C to study the effect of temperature.

A typical crystallization experiment is shown in Figure 4-1. The slurry density (mmole/liter) determined from the titration rate of Na_2SO_3 is plotted versus reaction time. The crystal growth rate is then calculated from the slope of the curve. Due to overshooting and fluctuation problems at the very beginning of some experiments, the crystal growth rates of all experiments were determined from the slope of the titration curves at the time when the slurry density has increased 50% relative to its initial value. The absolute growth rate was normalized by the BET surface area (N_2) of the initial seed.

The curve shown in Figure 4-1 is slightly concave upward. However, the slope change is small and the crystal growth rate is nearly independent of reaction time and crystal size/mass. The measured rates are two to three orders-of-magnitude slower than the

rates predicted by the mass transfer model developed in Chapter 3, that suggests calcium sulfite crystallization is not controlled by diffusion in the solution boundary layer.

SEM was used to characterize the shape and size of the crystal. Since calcium sulfite solids are not electrically conductive, the solids were sputtered or vacuum-evaporated with an alloy of Au and Pd to provide the necessary conducting medium for the SEM. IR was used to detect the presence of sulfate in the $\text{CaSO}_3 \cdot 1/2\text{H}_2\text{O}$ solids. The absorption structures of interest are the major sulfite band at approximately 990 cm^{-1} and the sulfate band near 1130 cm^{-1} . Peak heights of sulfite and sulfate absorption bands in the IR spectra were used to estimate the content of sulfate in the solids (Meserole, 1983).

4.5 Results and Discussion: Growth Rate

The experimental results are given in Table 4-3. Most of the data were obtained at $23\text{ }^\circ\text{C}$ with seed 1 at ionic strengths of 0.3 and 0.9 eq/l. Additional data were obtained at $55\text{ }^\circ\text{C}$ and with seeds 3 and 5.

4.5.1 Growth Rate Correlation

The growth rate, R' (mole/cm²-minute), was correlated as a function of calcium sulfite relative supersaturation, temperature, and gypsum saturation as follows:

$$R' = 9.7 \times 10^{-4} e^{-10250/RT} (RS_{\text{CaSO}_3} - 1)^2 RS_{\text{CaSO}_4}^{-1} \quad (3)$$

The $\text{CaSO}_3 \cdot 1/2\text{H}_2\text{O}$ crystal growth rate is second order relative to supersaturation, and is strongly inhibited by the presence of sulfate. The decrease of growth rate is 1st order relative to gypsum saturation.

4.5.2 Effect of Gypsum Saturation

The presence of dissolved sulfate reduces $\text{CaSO}_3 \cdot 1/2\text{H}_2\text{O}$ crystal growth significantly. In Figure 4-2, the growth rates with sulfate are normalized to the growth rate at the "zero sulfate" condition. The rate of $\text{CaSO}_3 \cdot 1/2\text{H}_2\text{O}$ crystal growth is inversely proportional to the gypsum saturation.

4.5.3 Effect of Temperature, Dissolved Sulfate and Seed Crystal Variation

The rate of crystal growth was measured with the three batches of seed crystals characterized by Table 4-1. The crystal growth rates per unit BET surface area are plotted versus relative supersaturation in Figure 4-3. It can be seen that $\text{CaSO}_3 \cdot 1/2\text{H}_2\text{O}$

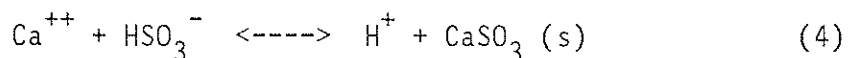
crystal growth rate is proportional to the second order of relative supersaturation, and the effects of temperature and gypsum saturation on crystal growth of the three seed crystals are the same. It also appears that BET surface area is better than particle size as a characteristic to distinguish seed crystals.

In Figure 4-3, temperature shows a strong effect on the growth rate. This result suggests $\text{CaSO}_3 \cdot 1/2\text{H}_2\text{O}$ crystal growth is controlled by surface kinetics, not by mass transfer which normally shows a less significant effect of temperature. The growth rate at 55 °C, as at 23 °C, is second order relative to supersaturation. The activation energy for $\text{CaSO}_3 \cdot 1/2\text{H}_2\text{O}$ crystal growth is estimated to be 10.3 kcal/gmole.

Another set of experimental data in Figure 4-3 were obtained with a gypsum saturation of 1.9. The crystal growth of $\text{CaSO}_3 \cdot 1/2\text{H}_2\text{O}$ at this high gypsum saturation has a steeper slope with respect to relative supersaturation.

4.5.4 Effects of pH, Solution Composition, Temperature, and Ionic Strength

At typical pH values of FGD, total dissolved sulfite is mostly bisulfite, so CaSO_3 equilibrium is a strong function of pH as given by



Relative supersaturation is also a function of dissolved Ca^{++} and total dissolved sulfite. Higher pH, higher Ca^{++} , and higher total sulfite all give increased rates of $\text{CaSO}_3 \cdot 1/2\text{H}_2\text{O}$ crystallization.

In Table 4-3, Two sets of experimental data were obtained at bulk solutions of high ionic strength (0.9 eq/l) and low ionic strength (0.3 eq/l) separately. In each set of experimental data, the solution composition varied while the ionic strength was kept the same. When CaCl_2 was substituted by an equivalent ionic strength of NaCl , the crystal growth dropped significantly due to the decrease of Ca^{++} activity which directly determines the solubility product of calcium sulfite. Therefore, a higher pH is needed to shift more HSO_3^- to $\text{SO}_3^{=}$ and thus increase the supersaturation to provide the driving force for crystal growth.

4.6 Results and Discussion: Crystal Habit

The grown crystals in the crystallization experiments were filtered, dried, and recovered for study of the crystal habit. Scanning electron microscopy and infrared spectroscopy have been used to examine the changes in crystal morphology and solid composition. Seed 1 was used in most of the experimental runs, seeds 3 and 5 were used to study the effect of seed crystal variation.

The effects of solution composition, ionic strength, temperature, gypsum saturation and seed crystal variation on $\text{CaSO}_3 \cdot 1/2\text{H}_2\text{O}$ crystal habit were studied. Substances whose chemical properties are similar to those of the crystallizing component often become habit modifiers (Toyokura, 1981), and this is the case for CaSO_4 , which has been found to be a strong habit modifier for $\text{CaSO}_3 \cdot 1/2\text{H}_2\text{O}$.

4.6.1 Effect of Gypsum Saturation

Calcium sulfate has a very strong effect on $\text{CaSO}_3 \cdot 1/2\text{H}_2\text{O}$ crystal habit. Because of solution sulfate impurities, none of the rate studies give the extreme of low CaSO_4 that gives large crystals in seed 5 (Figure 2-12). A dramatic change in crystal morphology was observed when the seeds were grown in a solution with 190 percent gypsum saturation (Figure 4-4) compared with that grown without sulfate in the solution (Figure 4-5). Agglomerates of very thin crystals were generated and IR spectroscopy indicated the increase of solid sulfate content. A probable explanation of this effect is that CaSO_4 selectively inhibits the growth of one crystal face as the other faces grow relatively more rapidly. The resulting crystal is a very thin platelet. This explanation is consistent with the earlier observation that CaSO_4 dramatically reduces the net rate of crystal growth.

4.6.2 Seed Crystal Variation

A comparison of the SEM photographs of the grown crystals from all three seeds suggests that the crystal habit of $\text{CaSO}_3 \cdot 1/2\text{H}_2\text{O}$ is mainly determined by the gypsum saturation, solution composition, and temperature; seed crystal variation has only a minor effect. It can be anticipated that if different seed crystals were grown in the same solution composition for quite a long time, identical growth rates and crystal habit would be observed no matter what kind of seed crystals they came from.

The SEM photograph in Figure 4-6 exhibits a dramatic change in the crystal habit of seed 5 as it was grown in a solution of high gypsum saturation. Thin crystals were obtained though the original seeds were thick. The SEM photograph of the partially grown crystals at 60 percent growth (Figure 4-7) shows clearly how the thick columnar hexagonal seed crystals were grown into thin crystals during the transition period of the dramatic change in crystal habit.

4.6.3 Effect of Solution Composition, Temperature and Ionic Strength

In the absence of CaSO_4 , the crystal habit does not change as a function of solution composition when the seed is grown in a high Ca^{++} environment, as shown in Figure 4-5 previously. However, crystals grow bulkier and thicker in Na^+ environment (Figure 4-8). Crystals grown at ionic strengths of 0.3 and 0.9 eq/l exhibit no

significant change in crystal morphology. Variation of temperature in the range of 23 to 55 °C shows no significant effect on $\text{CaSO}_3 \cdot 1/2\text{H}_2\text{O}$ crystal habit for most of the crystallization experiments.

Since seeds grow bulkier in Na^+ environment and thinner in $\text{SO}_4^{=}$ environment, the combination of these two effects was studied. The morphology of the grown crystals demonstrated that the effect of gypsum saturation overrides the effect of Na^+ (Figure 4-9).

4.8 Literature Cited

1. Acurex Corp., "Operation of EPA-Owned Pilot SO₂ Scrubber", Progress Report For January, 1984, EPA Contract 68-02-3648
2. Barkley, et al., "Evaluation of Sodium Thiosulfate Additive on the Performance of a Spray Tower Scrubber System Using Limestone Slurry", TVA/OP/EDT-84/7 (1983)
3. Borgwardt, R. H., "Proceedings: Symposium on Flue Gas Desulfurization", EPA Report 600/2-76-136a, 117 - 144 (1976)
4. Cares. R., Personal communication, M. W. Kellogg, Houston (1982)
5. Chan, P. K. and G. T. Rochelle, "Limestone Dissolution: Effects of pH, CO₂, and Buffers Modeled by Mass Transfer", ACS Symp. Ser., 188, 75 - 97 (1982)
6. Chang, C. S. and G. T. Rochelle, "SO₂ Absorption Into Aqueous Solutions", AIChE J. 27, 292 - 298 (1981)
7. Chang, C. S. and G. T. Rochelle, "Mass Transfer Enhanced by Equilibrium Reactions", Ind. Eng. Chem. Fundam. 21, 379 - 385 (1982)

8. Chang, C. S. and N. Kaplan, "Pilot Evaluation of Limestone Regenerated Dual Alkali Process", Presented at the EPA/EPRI Symposium on Flue Gas Desulfurization, New Orleans, November 1 - 4, 1983
9. Edwards, L. O. et al. "Calcium Sulfite Crystal Sizing Studies", EPA Report 600/7-79-192 (1979)
10. Erwin, J., Wang, C. C. and J. L. Hudson, "A Model of Oxidation in Calcium Sulfite Slurries", ACS Symp. Ser. 188, 191 - 220 (1982)
11. Glancy, D. L. et al., "Utility Double Alkali Operating Experience", Presented at FGD Symposium, New Orleans, November 1 - 4, 1983
12. Jones, B. F., Lowell, P. S., and F. B. Meserole, "Experimental and Theoretical Studies of solid Solution Formation in Lime and Limestone SO₂ Scrubbers", EPA Report 600/2-76-273a (1976)
13. Kelly, B., Keough, B., and A. D. Randolph, "Some Effects of Crystal Modifiers on CaSO₃·1/2H₂O Crystal Habit, Growth and Nucleation", Presented at AIChE National Meeting, Houston, March 27 - 31, 1983

14. Kerr, C. P. "Chemical Equilibria in Flue Gas Scrubbing Slurries", ACS Symp. Ser. 133, 93 - 106 (1980)
15. LaMantia, C. R. et al., "Proceedings: Symposium on Flue Gas Desulfurization-Atlanta", EPA-650/2-74-126a, 549 (1974)
16. Lowell, P. S. et al., "A Theoretical Description of The Limestone Injection - Wet Scrubbing Process", Radian Corporation (1970)
17. Meserole, F. B., Personal communication, Radian, Austin, 1983
18. Meserole, F. B., Trofe, T. W. and D. A. Stewart, "Influence of High Dissolved Solids on Precipitation Kinetics and Solid Particle Size", Presented at FGD Symposium, New Orleans, November 1 - 4, 1983
19. Meyer, B., "Sulfur, Energy, And Environment", Elsevier Scientific Publishing Co., Amsterdam, The Netherlands (1977)
20. Ottmers, D. et al. "A Theoretical and Experimental Study of The Lime/Limestone Wet Scrubbing Process", EPA Report 650/2-75-006 (1974)

21. Phillips, J. L. et al. "Development of a Mathematical Basis for Relating Sludge Properties to FGD-Scrubber Operating Variables", EPA Report 600/7-78-072 (1978)
22. Randolph, A. D. and D. Etherton, "Study of Gypsum Crystal Nucleation and Growth Rates in Simulated Flue Gas Desulfurization Liquors", EPRI Report CS-1885 (1981)
23. Rochelle, G. T. and C. J. King, "The Effect of Additives on Mass Transfer in CaO/CaCO₃ Slurry Scrubbing of SO₂ From Waste Gases", Ind. Eng. Chem. Fundam. 16, 67 - 75 (1977)
24. Rosenblatt, G. M. "Estimation of Activity Coefficients in Concentrated Sulfite-Sulfate Solutions", AIChE J. 27, 619 - 626 (1981)
25. Rowland, C. H., Abdulsattar, A. H., and D. A. Burbank, "Effects of Aqueous Chemical Equilibria on Wet Scrubbing of Sulfur Dioxide With Magnesia-Enhanced Limestone", ACS Symp. Ser. 133, 247 - 267 (1980)
26. Setoyama, K. and S. Takahashi, "Solid Solution of Calcium Sulfite Hemihydrate and Calcium Sulfate", Yogyo-Kyokai-shi 86, 56 - 62 (1978)

27. Toprac, A. J. and G. T. Rochelle, "Limestone Dissolution in Stack Gas Desulfurization Processes", Env. Prog. 1, 52 - 58 (1982)
28. Toyokura, K. "Encyclopedia of Chemical Processing and Design", edited by J. J. McKetta and W. A. Cunningham, 7, 407 - 420, M. Dekker Publisher, New York (1980)
29. Ulrich, R. K., Prada, R. E. and G. T. Rochelle, "Oxygen Absorption into Bisulfite Solutions Containing Single and Synergistic Metal Catalysts", Presented at the AIChE National Meeting, Houston, March 27 - 31, 1983
30. Wang, S. C., Personal communication, Bechtel, San Francisco, 1982

Chapter 5

Conclusions and Recommendations

5.1 Conclusions

1. The calcium sulfite solids were characterized to be $\text{CaSO}_3 \cdot 1/2\text{H}_2\text{O}$ using X-ray, DSC, IR, and iodometric titration.
2. No separate phase of calcium sulfate hemihydrate ($\text{CaSO}_4 \cdot 1/2\text{H}_2\text{O}$) or gypsum ($\text{CaSO}_4 \cdot 2\text{H}_2\text{O}$) was observed. The sulfate content in the calcium sulfite solids was incorporated in the $\text{CaSO}_3 \cdot 1/2\text{H}_2\text{O}$ crystal lattice.
3. The calcium sulfite solids are agglomerates of platelet or columnar crystals. The shape and platelet thickness is a strong function of sulfate content in the solids.
4. The dissolution of $\text{CaSO}_3 \cdot 1/2\text{H}_2\text{O}$ can be modelled successfully by mass transfer. The dissolution rate was

found to be controlled by the diffusion of H^+ , $SO_3^{=}/HSO_3^-$ and $CaSO_3^0$ ion pairs, not by surface reaction kinetics.

5. The stagnant mass transfer model underpredicts the dissolution rates. The observed values of Sherwood number (3.4 to 4.0) are expected with the particle size and shape observed.
6. The equilibrium pH for $CaSO_3 \cdot 1/2H_2O$ dissolution is determined by the dissolved Ca^{++} and $SO_3^{=}$ concentrations and the solubility of the $CaSO_3 \cdot 1/2H_2O$ solids.
7. The solubility of $CaSO_3 \cdot 1/2H_2O$ is a function of temperature and the sulfate content in the solids. It decreases as the temperature increases and increases as the solid sulfate content increases.
8. Dissolved sulfate in the aqueous solution strongly inhibits $CaSO_3 \cdot 1/2H_2O$ dissolution, probably by surface adsorption.
9. Dissolved Mg^{++} enhances the rate of $CaSO_3 \cdot 1/2H_2O$ dissolution by forming strong ion pairs with $SO_3^{=}$.
10. The crystal growth of $CaSO_3 \cdot 1/2H_2O$ is controlled by

surface kinetics, not by diffusion in a solution boundary layer.

11. The crystal growth rate is second order in $\text{CaSO}_3 \cdot 1/2\text{H}_2\text{O}$ supersaturation, and the estimated activation energy is 10 kcal/gmol.
12. Dissolved sulfate in aqueous solutions strongly inhibits the crystal growth of $\text{CaSO}_3 \cdot 1/2\text{H}_2\text{O}$. The rate of crystal growth is inversely proportional to the gypsum saturation.
13. Dissolved sulfate in the aqueous solution changes the crystal habit of $\text{CaSO}_3 \cdot 1/2\text{H}_2\text{O}$ from columnar to thin platelet. The dewatering properties of calcium sulfite solids from flue gas desulfurization processes should be enhanced by inhibiting sulfite oxidation.
14. Seed crystal variation has no significant effect on the ultimate $\text{CaSO}_3 \cdot 1/2\text{H}_2\text{O}$ crystal habit.

5.2 Recommendations for Further Work

1. Measure and model the dissolution and crystallization rate of $\text{CaSO}_3 \cdot 1/2\text{H}_2\text{O}$ in scrubbing solutions with organic acids and carbonate, because they may enhance or inhibit dissolution and crystal growth.
2. Study the effect of sulfite oxidation catalysts/inhibitors, such as Mn^{++} , Fe^{++} , and thiosulfate on the dissolution and crystal growth of calcium sulfite.
3. Check the validities of equilibrium constants, diffusivities, and activity coefficients of various species in the solution equilibrium program, especially at high ionic strength.
4. Use a continuous crystallizer to study CaSO_3 crystal growth and nucleation.
5. Develop an integrated SO_2 scrubber model which incorporates SO_2 absorption, CaCO_3 dissolution, sulfite oxidation, and CaSO_3 dissolution/crystallization.

6. Model the effect of sulfate on dissolution and crystal growth.
7. Study the dissolution and crystallization as a function of crystal size and habit, especially single platelets.

Appendix A.

X-ray Powder Diffraction Patterns
of The $\text{CaSO}_3 \cdot 1/2\text{H}_2\text{O}$ Seed Crystals

Appendix B.

Literature Values of The X-ray Powder Diffraction Patterns of Some Calcium Sulfite and Calcium Sulfate Compounds

Appendix C.

Derivation of The Stagnant Mass Transfer Model Surrounding A Single Particle

$$\begin{aligned}
 -dV/dt &= k_c \pi d_p^2 \Delta C / \rho_m \\
 &= (k_c d_p / D) D \pi d_p \Delta C / \rho_m \\
 &= Sh D \pi d_p \Delta C / \rho_m \\
 &= k V^{1/3}
 \end{aligned}$$

$$\text{where } k = Sh D \Delta C (6 \pi^2)^{1/3} / \rho_m$$

Assume Sh is not a function of particle size,

$$\text{integrate } -dV/dt = k V^{1/3}$$

$$V^{2/3} - V_o^{2/3} = -2/3 kt$$

$$\begin{aligned}
 V/V_o &= (1 - 2kt/3V_o^{2/3})^{1.5} \\
 &= (1 - k' t/d_p^2)^{1.5}
 \end{aligned}$$

$$\text{where } k' = 4 Sh D \Delta C / \rho_m$$

Assume a small spherical particle in a stagnant medium,

$$Sh \approx 2, \quad k' \approx 8 D \Delta C / \rho_m$$

Appendix D.

Tabulation of CaSO_3 Dissolution Rate Data

Appendix E.

Tabulation of CaSO_3 Crystal Growth Rate Data
in The Presence of Dissolved Mg^{++}

Appendix F.

Apparent pKa Values of HSO_3^- in Aqueous Solutions

Typical of FGD Processes

VITA

Chii-Huei Philip Tseng was born in Taiwan, Republic of China, on September 15, 1953, the son of Hsi-Pan Tseng and Yueh-Mei Chen. He entered the National Taiwan University in September, 1971, and graduated in June, 1975 with a degree of Bachelor of Science in Engineering. After two years of military service in the Chinese Army, he entered the National Tsing Hua University to pursue his graduate study and got his Master's degree in June, 1979. Then he worked for the Chinese Petroleum Corporation as a research engineer. In September, 1980, he entered the Graduate School of The University of Texas at Austin.

Permanent Address: 2F, No.3, Alley 6, Lane 212, Chung-Cheng Road
Shih-Lin, Taipei, Taiwan 111
Republic of China

This dissertation was typed by the author.